

# Scalable Bayesian Semiparametric Additive Regression Models For Microbiome Studies

Tinghua Chen

College of Information Science and Technology,  
Pennsylvania State University

and

Michelle Pistner Nixon

College of Information Science and Technology,  
Pennsylvania State University

and

Justin D. Silverman\*

College of Information Science and Technology,  
Department of Statistics,  
Department of Medicine,  
Pennsylvania State University

May 27, 2025

## Abstract

Statistical analysis of microbiome data is challenging. Bayesian multinomial logistic-normal (MLN) models have gained popularity due to their ability to account for the count compositional nature of these data, but existing approaches are either computationally intractable or restricted to purely parametric or non-parametric methods, which limit their flexibility and scalability. In this work, we introduce *Multi-AddGPs*, a novel semi-parametric framework that integrates additive Gaussian Process (GP) regression within a Bayesian MLN model to disentangle linear and non-linear covariate effects, including non-stationary dynamics. Our approach builds on the computationally efficient Collapse-Uncollapse (CU) sampler and additive GP regression, introducing a novel back-sampling algorithm and marginal likelihood approximation for efficient inference and hyperparameter estimation. Our models are over 240,000 times faster than alternatives while simultaneously producing more accurate posterior estimates. Additionally, we incorporate non-stationary kernel functions designed to model treatment interventions and disease effects. We demonstrate our approach using

---

\*The authors gratefully acknowledge Rachel Silverman and Hangzhi Guo for their helpful comments. This work was supported by the NIH under Grant 1 R01 GM148972-01.

simulated and real data studies and produce novel biological insights from a previously published human gut microbiome study. Our methods are publicly available as part of the *fido* software package on CRAN <sup>1</sup>.

*Keywords:* Additive Regression, Multinomial Logistic-Normal Models, Bayesian Inference, Microbiome Data, Gaussian Process

## 1 Introduction

Dysregulation of human-, animal-, and even plant-associated microbial communities (microbiota) are known to cause disease (Ballen et al. 2016, Frati et al. 2018, Holleran et al. 2018, Sharon et al. 2019, Gao et al. 2021). In humans, alterations of microbiota play a causal role in obesity (Tilg et al. 2011, Ley 2010), inflammatory bowel disease (Honda & Littman 2012, Glassner et al. 2020, Kostic et al. 2014), and even cancer (Schwabe & Jobin 2013, Helmink et al. 2019). As a result, many researchers study how dietary, host physiologic, and environmental factors influence the relative abundance of different bacterial taxa in microbiota. These factors can have linear or non-linear effects on community structure (Cheng et al. 2019, Sankaran & Jeganathan 2024, Schwager et al. 2017). Even within closed *in vitro* systems, microbiota can demonstrate non-linear temporal variation (Silverman et al. 2018). While additive regression models have been proposed to model these complexities, existing implementations are too computationally intensive for widespread use and ignore the count compositional nature of these data (Timonen et al. 2021, Cheng et al. 2019). Overall, interpretable and flexible statistical methods are needed to disentangle and infer linear and non-linear effects on microbiota.

Limitations of the sequence counting measurement process complicate the analysis of microbiome data. These data are typically represented as a  $D \times N$  count table  $Y$  with elements  $Y_{dn}$  denoting the number of DNA molecules from taxon  $d$  observed (sequenced)

---

<sup>1</sup>A preliminary version of this work was presented at the NeurIPS 2024 Workshop on “Bayesian Decision-making and Uncertainty,” but was not published in the workshop proceedings.

in sample  $n$ . Critically, the counts  $Y_{dn}$  do not represent the true abundance of taxon  $d$  in the biological system (e.g., colon) from which the sample  $n$  was obtained. Instead, the counts are the results of a random sample of that pool of microbes. Due to limitations of the measurement process, the size of that sample (the sequencing depth;  $\sum_{d=1}^D Y_{dn}$ ) is typically arbitrary and unrelated to the total microbial load in the system (Vandeputte et al. 2017). As a result, many authors call these data compositional, reflecting the idea that the data only provide information about the relative abundances of the different taxa within each community (Gloor et al. 2017, McGregor et al. 2023, Mao & Ma 2022). However, unlike traditional compositional data (e.g., continuous simplex valued data), these data are zero-laden counts. The presence of counting noise and zeros limits standard approaches to compositional data analysis, which typically involve analyses of log-ratio transformed data (Kuczynski et al. 2012, Silverman et al. 2018, 2017, 2020, Kaul et al. 2017, Li 2015, Gloor et al. 2016).

A growing number of researchers are adopting Bayesian Multinomial Logistic Normal (MLN) models to tackle the challenges associated with the measurement process (Silverman et al. 2021, Äijö et al. 2018, Grantham et al. 2020, Silverman et al. 2018, 2022, Saxena et al. 2024). The multinomial component addresses uncertainty stemming from random counts, while the logistic normal component accounts for the extra-multinomial variability often observed in these datasets (Silverman et al. 2022). Furthermore, the multinomial framework provides a more intuitive representation of the generating process behind the numerous zero counts than traditional univariate zero-inflated models (Silverman et al. 2020). Conceptually, Bayesian MLN models allow researchers to represent community composition as a latent simplicial vector informed by the observed count data. In contrast to the more commonly used Dirichlet distribution, the logistic-normal distribution offers a rich covariance structure that facilitates the modeling of both positive and negative covariation among taxa (Aitchison

& Shen 1980, Silverman et al. 2018). The logistic-normal distribution is self-conjugate (as it forms a multivariate normal distribution under a suitable log-ratio transformation), permitting the construction of a diverse range of models within the latent simplex space. Although Multinomial-logistic normals have historically posed computational challenges that hinder widespread application, recent innovations, such as the Collapse-Uncollapse (CU) Sampler (Silverman et al. 2022), have addressed this limitation. Nevertheless, there is still a need for more flexible approaches that can effectively disentangle linear and non-linear effects as existing methods do not allow for additive linear and non-linear modeling (Silverman et al. 2022).

In this study, we introduce *MultiAddGPs*, a versatile and interpretable semi-parametric framework aimed at addressing key challenges in microbiome data analysis. MultiAddGPs are scalable Bayesian MLN models that facilitate additive combinations of both linear and non-linear Gaussian process components. Our approach demonstrates exceptional computational efficiency and scalability, outperforming existing alternatives by a factor of over 400 while yielding more accurate posterior estimates. Our inference algorithms leverage the CU Sampler from Silverman et al. (2022), while simultaneously enhancing those methods. We introduce a novel back-sampling algorithm for efficient posterior simulation from multivariate additive Gaussian process models as well as non-stationary kernels for estimation of non-linear intervention effects on complex microbial communities.

Moreover, we introduce an accurate and efficient method for marginal likelihood estimation that leverages the Laplace approximation within the CU sampler. Our marginal likelihood estimation procedure is critical as it allow for efficient hyperparameter estimation for MultiAddGPs as well as the broader class of models that can be sampled by the CU sampler (Silverman et al. 2022). We validate our methods through simulation and real data studies. We demonstrate that MultiAddGPs can directly estimate complex, time-lagged

effects of interventions on human microbiota. In an application involving an *ex vivo* artificial human gut study, our findings offer the first evidence that microbiota communities display oscillatory-like behavior in response to short-term dietary interventions.

	<i>MultiAddGPs</i>		<i>MLTPs</i>		<i>Lgpr</i>	<i>LongGP</i>
Model	Linear <b>and</b> Nonlinear	Linear <b>or</b> Nonlinear	Nonlinear	Nonlinear	Nonlinear	Nonlinear
Flexible Kernels	✓	✓	×	×	×	×
Scalable	✓	✓	×	×	×	×
Hyperparameter Estimation	✓	×	✓	✓	✓	✓
Count Compositional	✓	✓	×	×	×	×

Table 1: **A comparison of MultiAddGPs and existing alternatives.** MultiAddGPs (this article) facilitate additive modeling of both linear and non-linear processes. In contrast, MLTPs (Silverman et al. 2022) consist of either a single linear or a single non-linear component. The Lgpr (Timonen et al. 2021) and LongGP (Cheng et al. 2019) frameworks permit only additive non-linear components. Both MultiAddGPs and MLTPs are implemented in the *fido* software package available on CRAN, offering both pre-defined and user-defined kernels. Conversely, the Lgpr and LongGP packages restrict usage to pre-defined kernels. MultiAddGPs and MLTPs are computationally efficient due to the CU Sampler, while LongGP and Lgpr are computationally intensive and do not scale effectively to the datasets analyzed in this article. Notably, the MLTPs proposed by Silverman et al. (2022) lack a mechanism for estimating model hyperparameters, a feature present in the other three methods. Furthermore, MultiAddGPs and MLTPs address the count compositional nature of the data using Bayesian MLN models, whereas Lgpr is limited to univariate likelihoods, and LongGP assumes the data follows a Gaussian distribution.

## Notation

In this article, we denote matrix and vector dimensions with unbolded uppercase letters (e.g.,  $N$ ), matrices and matrix-valued functions using bold uppercase symbols (e.g.,  $\mathbf{X}$ ), vectors and vector-valued functions with bold lowercase symbols (e.g.,  $\mathbf{x}$ ), and scalars and scalar functions as unbolded lowercase symbols (e.g.,  $x$ ). For matrices, we index specific rows as  $\mathbf{X}_d$  and columns as  $\mathbf{X}_n$ . We denote vector-valued stochastic processes using the same notation as matrices (e.g.  $\mathbf{Y}$ ) since, in practice, we only evaluate these at a finite number of test points.

## 2 Methods

### 2.1 Multinomial Logistic Normal Additive Gaussian Process Models (MultiAddGPs)

Let  $\mathbf{Y}_n$  denote a  $D$ -vector of observed data,  $\mathbf{X}_n$  a  $Q_0$ -vector of covariates to model linearly, and each  $\mathbf{Z}_n^{(k \in \{1, \dots, K\})}$  a  $Q_k$ -vector of covariates to be modeled with distinct non-linear functions. The MultiAddGPs model have the following form:

$$\mathbf{Y}_n \sim \text{Multinomial}(\mathbf{\Pi}_n) \tag{1}$$

$$\mathbf{\Pi}_n = \phi^{-1}(\mathbf{H}_n) \tag{2}$$

$$\mathbf{H}_n \sim \mathcal{N}(\mathbf{F}_n, \mathbf{\Sigma}) \tag{3}$$

$$\mathbf{F} = \mathbf{B}\mathbf{X} + \sum_{k=1}^K \mathbf{f}^{(k)}(\mathbf{Z}^{(k)}) \tag{4}$$

with priors  $\mathbf{B} \sim \mathcal{N}(\mathbf{\Theta}^{(0)}, \mathbf{\Sigma}, \mathbf{\Gamma}^{(0)})$ ,  $\mathbf{f}^{(k)} \sim \mathcal{GP}(\mathbf{\Theta}^{(k)}, \mathbf{\Sigma}, \mathbf{\Gamma}^{(k)})$ , and  $\mathbf{\Sigma} \sim \mathcal{IW}(\mathbf{\Xi}, \zeta)$ . Here, the likelihood is  $p(\mathbf{Y}_{.1}, \dots, \mathbf{Y}_{.N}) \sim \prod_{n=1}^N \text{Multinomial}(\mathbf{\Pi}_n)$ ,  $\mathbf{\Sigma}$  is a  $(D-1) \times (D-1)$  covariance matrix, and the transform  $\phi$  is an invertible log-ratio transform from the  $D$ -dimensional simplex to  $D-1$  dimensional real-space:  $\mathbf{H}_n = \phi(\mathbf{\Pi}_n \in \mathbb{S}^D) \in \mathbb{R}^{D-1}$ . For computational

efficiency, we used the following Additive Log-Ratio (ALR) transform, which takes the  $D$ -th taxa as a reference:

$$\mathbf{H}_{.n} = \phi(\mathbf{\Pi}_{.n}) = \left\{ \log \left( \frac{\pi_{1n}}{\pi_{Dn}} \right), \dots, \log \left( \frac{\pi_{(D-1)n}}{\pi_{Dn}} \right) \right\}^T.$$

There is no loss of generality as posterior samples taken with respect to the  $\text{ALR}_D$  coordinate system can be transformed into any other log-ratio coordinate system (Pawłowsky-Glahn et al. 2015, Appendix A.3). For context, the  $\text{ALR}_D$  transform is the inverse of the identified softmax transform.

For the matrix-normal prior on the linear term,  $\Theta^{(0)}$  is the mean matrix and  $\Gamma^{(0)}$  is a  $Q_0 \times Q_0$  covariance matrix representing covariance in the parameters of the  $Q_0$  covariates. The terms  $\Theta^{(k)}$  and  $\Gamma^{(k)}$  in the  $K$  matrix-normal process priors echo their linear counterparts but are functions (e.g., mean and kernel functions) rather than fixed dimensional matrices. Additionally, we permit hyperparameters  $\Omega$  in any part of the model, including but not limited to hyperparameters in the kernel functions (e.g., bandwidth parameters) or hyperparameters in the mean functions.

As we will show through simulated and real data analyses in Sections 3 and 4, this is a very flexible class of models which can be used in a wide range of additive linear and non-linear modeling tasks.

## 2.2 Posterior Estimation in MultiAddGPs

We develop scalable inference for MultiAddGPs using a two-step Collapse-Uncollapse (CU) sampler (Silverman et al. 2022). Any multi-parameter Bayesian model  $p(\mathbf{H}, \Phi \mid \mathbf{Y})$  can be sampled in two-step: (1) obtain a sample from the marginal  $p(\mathbf{H} \mid \mathbf{Y})$  (the *collapse* step); (2) conditioned on that sample, obtain a sample from the corresponding conditional  $p(\Phi \mid \mathbf{H}, \mathbf{Y})$  (the *uncollapse* step). Yet this approach is often infeasible as these posterior marginals and conditionals are rarely available for non-conjugate models. Full details on

---

**Algorithm 1** The Collapse-Uncollapse (CU) Sampler for **MultiAddGPs** Models

---

**Input:** Data  $\{\mathbf{Y}, \mathbf{X}, \mathbf{Z}^{(1)}, \dots, \mathbf{Z}^{(K)}\}$ <sup>2</sup>, and prior parameters

$$\Delta = \{\Theta^{(0)}, \dots, \Theta^{(K)}, \Gamma^{(0)}, \dots, \Gamma^{(K)}, \Xi, \zeta\}.$$

**Output:**  $S$  samples of  $\{\mathbf{H}, \Sigma, \mathbf{F}, \mathbf{B}, \mathbf{f}^{(1)}, \dots, \mathbf{f}^{(K)}\}$ .

- 1: **for** each sample  $s \in \{1, \dots, S\}$  **do**
  - 2:     Sample  $\mathbf{H}^{[s]} \sim p(\mathbf{H}|\mathbf{Y}, \Delta)$  where  $p(\mathbf{H}, \mathbf{Y}, \Delta)$  is an LTP; ▷ Collapsed Step
  - 3:     Sample  $\{\Sigma^{[s]}, \mathbf{F}^{[s]}\} \sim p(\mathbf{F}, \Sigma | \mathbf{H}^{[s]}, \Delta)$ ; ▷ Uncollapsed Step (1)
  - 4:     Sample  $\mathbf{B}^{[s]}, \mathbf{f}^{(1)[s]}, \dots, \mathbf{f}^{(K)[s]} = \text{Back-Sampling}(\mathbf{Y}, \mathbf{F}^{[s]}, \Sigma^{[s]}, \Delta)$ ; ▷ Uncollapsed Step (2)
  - 5: **end for**
- 

the CU sampler can be found in Supplementary Section 1. [Silverman et al. \(2022\)](#) showed that there was a large class of semi-conjugate models called *Marginally Latent matrix-T Processes (MLTPs)* where, the posterior conditional  $p(\Phi | \mathbf{H}, \mathbf{Y})$  had a closed form and the posterior marginal  $p(\mathbf{H} | \mathbf{Y})$  was the posterior of a *Latent matrix-T Process (LTP)* which could be accurately and efficiently sampled through a Laplace approximation. Below we show that MultiAddGPs are MLTPs and derive the parameters of their marginal LTP form. These results, are used to form the Laplace approximation to the Collapse step for MultiAddGPs. We then derive a novel *Back-sampling (BS)* for multivariate additive Gaussian process regression models. The BS algorithm provides a closed-form solution for the Uncollapse step for MultiAddGPs. Finally, we develop efficient hyperparameter inference for MLTPs (including MultiAddGPs) by maximum marginal likelihood estimation and discuss the identification of posterior samples from MultiAddGPs.

### 2.2.1 MultiAddGPs as MLTPs and the Collapse Step

Just as Gaussian processes can be defined based on the marginal properties of the multivariate normal, matrix normal processes and matrix-t processes can be defined by the marginal

---

<sup>2</sup>We omit conditioning on covariates  $\mathbf{X}$  and  $\mathbf{Z}$  in the notation for brevity.

properties of the matrix normal and matrix-t distributions (Silverman et al. 2022). Matrix-t processes generalize Student-t processes and Gaussian processes (Silverman et al. 2022).

*Definition 2.1* (Matrix-T Process). A stochastic process  $\mathbf{Y} \sim TP(\nu, \mathbf{M}, \mathbf{V}, \mathbf{A})$  defined on the set  $\mathcal{W} = \mathcal{W}^{(1)} \times \mathcal{W}^{(2)}$  is a matrix-T process if  $\mathbf{Y}$  evaluated on any two finite subsets  $\mathcal{X}^{(1)} \subset \mathcal{W}^{(1)}$  and  $\mathcal{X}^{(2)} \subset \mathcal{W}^{(2)}$  is a random matrix of dimension  $|\mathcal{X}^{(1)}| \times |\mathcal{X}^{(2)}|$  that follows a matrix-T distribution:  $\mathbf{Y} \sim T(\nu, \mathbf{M}, \mathbf{V}, \mathbf{A})$ .  $\nu$  is a scalar value strictly greater than zero. Let  $x_i^{(1)}, x_j^{(1)} \in \mathcal{X}^{(1)}$  and  $x_i^{(2)}, x_j^{(2)} \in \mathcal{X}^{(2)}$ .  $\mathbf{M}_{ij} = \mathbf{M}(x_i^{(1)}, x_j^{(2)})$  is the matrix function representing the mean, and  $\mathbf{V}_{ij} = \mathbf{V}(x_i^{(1)}, x_j^{(1)})$  and  $\mathbf{A}_{ij} = \mathbf{A}(x_i^{(2)}, x_j^{(2)})$  are kernel functions. Latent Matrix-T Processes (LTP) generalize Matrix-T processes.

*Definition 2.2* (Latent Matrix-T Processes).  $\mathbf{Y}$  is said to be an LTP if

$$\begin{aligned}\mathbf{Y} &\sim g(\mathbf{\Pi}) \\ \mathbf{\Pi} &= \phi^{-1}(\mathbf{H}) \\ \mathbf{H} &\sim TP(\nu, \mathbf{M}, \mathbf{V}, \mathbf{A}).\end{aligned}$$

where  $g$  is any distribution depending on parameters  $\mathbf{\Pi}$  and  $\phi$  is a known transform.

A stochastic process  $\mathbf{Y}$  is Marginally LTP (MLTP) if there exists a joint distribution  $p(\mathbf{Y}, \mathbf{H}, \mathbf{\Phi})$  such that the marginal  $p(\mathbf{Y}, \mathbf{H})$  is a LTP. In Supplementary Section 2, we prove the following theorem, which establishes that MultiAddGPs are MLTPs.

**Theorem 2.3.** *MultiAddGPs are MLTPs with parameters  $\mathbf{\Phi} = \{\mathbf{F}, \mathbf{B}, \mathbf{f}^{(1)}, \dots, \mathbf{f}^{(K)}, \mathbf{\Sigma}\}$ .*

*The collapsed form  $p(\mathbf{Y}, \mathbf{H})$  is an LTP:*

$$\begin{aligned}\mathbf{Y}_{\cdot n} &\sim \text{Multinomial}(\mathbf{\Pi}_{\cdot n}) \\ \mathbf{\Pi}_{\cdot n} &= \phi^{-1}(\mathbf{H}_{\cdot n}) \\ \mathbf{H} &\sim TP(\nu, \mathbf{M}, \mathbf{V}, \mathbf{A})\end{aligned}$$

where  $\phi$  is an invertible log-ratio transformation,  $\mathbf{M} = \Theta^{(0)}\mathbf{X} + \sum_{k=1}^K \Theta^{(k)}(\mathbf{Z}^{(k)})$ ,  $\mathbf{V} = \Xi$ , and  $\mathbf{A} = \mathbf{X}^T \Gamma^{(0)} \mathbf{X} + \sum_{k=1}^K \Gamma^{(k)}(\mathbf{Z}^{(k)}) + \mathbf{I}_N$ ,  $\nu = \zeta$

In the collapsed step of the CU sampler, we approximate  $p(\mathbf{H} \mid \mathbf{Y})$  using a Laplace approximation:  $q(\mathbf{H} \mid \mathbf{Y}) = \mathcal{N}(\text{vec}(\hat{\mathbf{H}}), \nabla^{-2}(\text{vec}(\hat{\mathbf{H}})))$ , where  $\hat{\mathbf{H}}$  is the maximum a posteriori (MAP) estimate of  $p(\mathbf{H} \mid \mathbf{Y})$ , and  $\nabla^{-2}(\text{vec}(\hat{\mathbf{H}}))$  is the inverse Hessian of  $\log p(\mathbf{H} \mid \mathbf{Y})$  evaluated at  $\hat{\mathbf{H}}$ .

We obtain efficient MAP estimates  $\hat{\mathbf{H}}$  by applying the L-BFGS optimizer to the closed-form gradients  $\nabla(\text{vec}(\hat{\mathbf{H}}))$  derived in Supplementary Section 3. Building on these results, we then compute the Hessian  $\nabla^{-2}(\text{vec}(\hat{\mathbf{H}}))$  in closed form (also see Supplementary Section 3). This approximation is computationally efficient and extremely accurate. The error in this approximation is bounded in probability by  $O_p([D - 1] \sum_{n=1}^N \lambda_n^{-1})$  where  $\lambda_n = \sum_{d=1}^D \mathbf{Y}_{dn}$  (See Proposition 11 of Silverman et al. (2022)). This bound explains the high accuracy of the approximation in sequence count applications, such as microbiome data analysis, where the sequencing depth  $\lambda_n$  is typically large.

### 2.2.2 Back-sampling and the Uncollapse Step for MultiAddGPs

Each posterior sample from  $p(\mathbf{H}, \mid \mathbf{Y})$  is then conditioned upon and used to sample from  $p(\Phi \mid \mathbf{H}, \mathbf{Y})$  where  $\Phi = \{\mathbf{F}, \mathbf{B}, \mathbf{f}^{(1)}, \dots, \mathbf{f}^{(K)}, \Sigma\}$ . Since  $\Phi$  is conditionally independent of  $\mathbf{Y}$  given  $\mathbf{H}$  ( $\Phi \perp \mathbf{Y} \mid \mathbf{H}$ ), the uncollapse step simplifies to deriving an efficient sampler for  $p(\Phi \mid \mathbf{H})$ . Further, using the fact that  $\{\mathbf{B}, \mathbf{f}^{(1)}, \dots, \mathbf{f}^{(K)}\} \perp \mathbf{H} \mid \{\mathbf{F}, \Sigma\}$  we can break the uncollapse step into two simpler steps, with the second conditioned on the results of the first: (1) sample  $p(\Sigma, \mathbf{F} \mid \mathbf{H})$  and (2) sample  $p(\mathbf{B}, \mathbf{f}^{(1)}, \dots, \mathbf{f}^{(K)} \mid \mathbf{F}, \Sigma)$ .

Before proceeding, we must clarify the distinction between the set of observed data points  $n \in \{1, \dots, N\}$ , where the response  $\mathbf{Y}$  is observed, and the evaluation set  $n^* \in \{1, \dots, N^*\}$ , where the functions  $\mathbf{F}, \mathbf{B}_0, \mathbf{f}^{(1)}, \dots, \mathbf{f}^{(K)}$  are to be inferred. In what follows, we use the symbols

$\mathbf{F}, \mathbf{B}_0, \mathbf{f}^{(1)}, \dots, \mathbf{f}^{(K)}$  to denote the evaluation of corresponding infinite-dimensional functions at the set of evaluation points  $\{1, \dots, N^*\}$ , i.e., they are each  $D \times N^*$ -dimensional random matrices. In contrast, all other random matrices (e.g.,  $\mathbf{H}$ ) represent their corresponding infinite-dimensional analogues evaluated at the set of observed points  $\{1, \dots, N\}$ .

**2.2.2.1 Sampling  $p(\Sigma, \mathbf{F} \mid \mathbf{H})$**  Conditioning on  $\mathbf{H}$  and marginalizing over  $\mathbf{f}^{(k)}, k \in \{1, \dots, K\}$  in the MultiAddGPs model results in a Bayesian matrix-normal process model with likelihood  $\mathbf{H}_n \sim \mathcal{N}(\mathbf{F}_n, \Sigma)$  and priors:

$$\mathbf{F} \sim \mathcal{GP} \left( \Theta^{(0)} \mathbf{X} + \sum_{k=1}^K \Theta^{(k)}(\mathbf{Z}^{(k)}), \Sigma, \mathbf{X}^T \Gamma^{(0)} \mathbf{X} + \sum_{k=1}^K \Gamma^{(k)}(\mathbf{Z}^{(k)}) \right)$$

$$\Sigma \sim \mathcal{IW}(\Xi, \zeta).$$

This model is conjugate and posterior samples of  $\mathbf{F}$  and  $\Sigma$  can be efficiently obtained as described in Supplementary Section 2.2.

**2.2.2.2 Sampling  $p(\mathbf{B}, \mathbf{f}^{(1)}, \dots, \mathbf{f}^{(K)} \mid \mathbf{F}, \Sigma)$  via Back-sampling** Inspired by the backfitting algorithm used in generalized additive models (Wood 2017), we introduce a novel *Back-sampling (BS)* algorithm which iteratively smooths (i.e., decomposes)  $\mathbf{F}$  into additive components.

For each posterior sample, the BS algorithm proceeds by sampling  $p(\mathbf{B} \mid \mathbf{F}, \Sigma)$  and then sequentially sampling  $p(\mathbf{f}^{(1)} \mid \mathbf{B}, \mathbf{F}, \Sigma), \dots, p(\mathbf{f}^{(K-1)} \mid \mathbf{f}^{(1)}, \dots, \mathbf{f}^{(K-2)}, \mathbf{B}, \mathbf{F}, \Sigma)$ . Note the value of the final  $\mathbf{f}^{(K)}$  is uniquely determined by the values of  $\mathbf{F}, \mathbf{B}, \mathbf{f}^{(1)}, \dots, \mathbf{f}^{(K-1)}$  and so a sample of  $\mathbf{f}^{(K)}$  from the joint distribution can be obtained by calculating  $\mathbf{f}^{(K)} = \mathbf{F} - \mathbf{B}\mathbf{X} - \mathbf{f}^{(1)} - \dots - \mathbf{f}^{(K-1)}$ . The pseudocode for the BS algorithm is provided in Algorithm 2.

First we sample from the posterior  $p(\mathbf{B} \mid \mathbf{F}, \Sigma)$ . To do this we marginalize over  $\mathbf{f}^{(1)}, \dots, \mathbf{f}^{(K)}$  and reparameterize as  $\mathbf{B}^\epsilon := \mathbf{F} - \sum_{k=1}^K \Theta^{(k)}(\mathbf{Z}^{(k)})$ .

This leads to the following conjugate Bayesian model for  $\mathbf{B}$ :

$$\mathbf{B}^\epsilon \sim \mathcal{MN}(\mathbf{B}\mathbf{X}, \boldsymbol{\Sigma}, \boldsymbol{\Gamma}^*)$$

$$\mathbf{B} \sim \mathcal{MN}(\boldsymbol{\Theta}^{(0)}, \boldsymbol{\Sigma}, \boldsymbol{\Gamma}^{(0)})$$

where  $\boldsymbol{\Gamma}^* = \sum_{k=1}^K \boldsymbol{\Gamma}^{(k)}(\mathbf{Z}^{(k)})$ , and  $\boldsymbol{\Theta}^{(0)}$ ,  $\boldsymbol{\Gamma}^{(0)}$  denote the prior mean and covariance of  $\mathbf{B}$ , respectively. Using Supplementary Section 4, we have the following closed form for the posterior:

$$\mathbf{B} \mid \mathbf{B}^\epsilon, \boldsymbol{\Sigma} \sim \mathcal{MN}\left(\left[\mathbf{B}^\epsilon \boldsymbol{\Gamma}^{-*} \mathbf{X}^T + \boldsymbol{\Theta}^{(0)} \boldsymbol{\Gamma}^{-(0)}\right] \left[\mathbf{X} \boldsymbol{\Gamma}^{-*} \mathbf{X}^T + \boldsymbol{\Gamma}^{-(0)}\right]^{-1}, \boldsymbol{\Sigma}, \left[\mathbf{X} \boldsymbol{\Gamma}^{-*} \mathbf{X}^T + \boldsymbol{\Gamma}^{-(0)}\right]^{-1}\right)$$

where  $\boldsymbol{\Gamma}^{-*} = (\boldsymbol{\Gamma}^*)^{-1}$  and  $\boldsymbol{\Gamma}^{-(0)} = (\boldsymbol{\Gamma}^{(0)})^{-1}$ .

We use a similar trick to sample each nonlinear component  $p(\mathbf{f}^{(1)} \mid \mathbf{B}, \mathbf{F}, \boldsymbol{\Sigma}), \dots, p(\mathbf{f}^{(K-1)} \mid \mathbf{f}^{(1)}, \dots, \mathbf{f}^{(K-2)}, \mathbf{B}, \mathbf{F}, \boldsymbol{\Sigma})$ . For each  $k \in \{1, \dots, K-1\}$ , we reparameterize the model as:  $\mathbf{f}^{\epsilon_k} = \mathbf{F} - \mathbf{B}\mathbf{X} - \sum_{i=1}^{k-1} \mathbf{f}^{(i)} - \sum_{j=k+1}^K \boldsymbol{\Theta}^{(j)}(\mathbf{Z}^{(j)})$ . Similar to  $\mathbf{B}^\epsilon$ ,  $\mathbf{f}^{\epsilon_k}$  leads to the following conjugate Bayesian model for each  $\mathbf{f}^{(k)}$ :

$$\mathbf{f}^{\epsilon_k} \sim \mathcal{MN}(\mathbf{f}^{(k)}, \boldsymbol{\Sigma}, \boldsymbol{\Gamma}^*)$$

$$\mathbf{f}^{(k)} \sim \mathcal{GP}(\boldsymbol{\Theta}^{(k)}, \boldsymbol{\Sigma}, \boldsymbol{\Gamma}^{(k)})$$

where  $\boldsymbol{\Gamma}^* = \sum_{j=k+1}^K \boldsymbol{\Gamma}^{(j)}$ . Again, this can be sampled in closed form using the results of Supplementary Section 4:

$$\mathbf{f}^{(k)} \mid \boldsymbol{\Sigma}, \mathbf{f}^{\epsilon_k} \sim \mathcal{MN}\left(\left[\mathbf{f}^{\epsilon_k} \boldsymbol{\Sigma}^{-*} + \boldsymbol{\Theta}^{(k)} \boldsymbol{\Gamma}^{-(k)}\right] \left[\boldsymbol{\Gamma}^{-*} + \boldsymbol{\Gamma}^{-(k)}\right]^{-1}, \boldsymbol{\Sigma}, \left[\boldsymbol{\Gamma}^{-*} + \boldsymbol{\Gamma}^{-(k)}\right]^{-1}\right)$$

where  $\boldsymbol{\Gamma}^{-*}$  and  $\boldsymbol{\Gamma}^{-(k)}$  are short-hand for  $(\boldsymbol{\Gamma}^*)^{-1}$  and  $(\boldsymbol{\Gamma}^{(k)})^{-1}$  respectively.

Finally, the last component  $\mathbf{f}^{(K)}$  is uniquely determined as:  $\mathbf{f}^{(K)} = \mathbf{F} - \mathbf{B}\mathbf{X} - \sum_{k=1}^{K-1} \mathbf{f}^{(k)}$

## 2.3 Model Identification

Function decomposition models like MultiAddGPs or generalized additive models may not be fully identified (Hastie 2017). Whereas this poses a fundamental problem for Frequentist

---

**Algorithm 2** Back-sampling (BS)

---

**Input:**  $\{\mathbf{Y}, \mathbf{X}, \mathbf{Z}\}$  are data observations;  $\{\mathbf{F}, \Sigma\}$  are samples from the uncollapsed step (1);

$\Delta = \{\Theta^{(0)}, \dots, \Theta^{(K)}, \Gamma^{(0)}, \dots, \Gamma^{(K)}\}$  is a set of prior inputs.

**Output:**  $S$  samples of the form  $\{\mathbf{B}, \mathbf{f}^{(1)}, \dots, \mathbf{f}^{(K)}\}$

- 1: **for**  $s = 1$  to  $S$  **do**
  - 2:      $\mathbf{B}^\epsilon = \mathbf{F} - \sum_{k=1}^K \Theta^{(k)}(\mathbf{Z}^{(k)})$
  - 3:      $\Gamma^* = \sum_{k=1}^K \Gamma^{(k)}$
  - 4:      $\mathbf{B} | \mathbf{B}^\epsilon, \Sigma \sim \mathcal{MN} \left( \left[ \mathbf{B}^\epsilon \Gamma^{*-} \mathbf{X}^T + \Theta^{(0)} \Gamma^{-(0)} \right] \left[ \mathbf{X} \Gamma^{*-} \mathbf{X}^T + \Gamma^{-(0)} \right]^{-1}, \Sigma, \left[ \mathbf{X} \Gamma^{*-} \mathbf{X}^T + \Gamma^{-(0)} \right]^{-1} \right)$
  - 5:     **for**  $k = 1$  to  $K$  **do**
  - 6:          $\mathbf{f}^{\epsilon_k} = \mathbf{F} - \mathbf{B} \mathbf{X} - \sum_{i=1}^{k-1} \mathbf{f}^{(i)} - \sum_{j=k+1}^K \Theta^{(j)}(\mathbf{Z}^{(j)})$
  - 7:          $\Gamma^* = \sum_{j=k+1}^K \Gamma^{(j)}$
  - 8:          $\mathbf{f}^{(k)} | \Sigma, \mathbf{f}^{\epsilon_k} \sim \mathcal{MN} \left( \left[ \mathbf{f}^{\epsilon_k} \Sigma^{*-} + \Theta^{(k)} \Gamma^{-(k)} \right] \left[ \Gamma^{*-} + \Gamma^{-(k)} \right]^{-1}, \Sigma, \left[ \Gamma^{*-} + \Gamma^{-(k)} \right]^{-1} \right)$
  - 9:     **end for**
  - 10:      $\mathbf{f}^{(K)} = \mathbf{F} - \mathbf{B} \mathbf{X} - \sum_{k=1}^{K-1} \mathbf{f}^{(k)}$
  - 11: **end for**
- 

procedures, this form of partial identifiability can provide important information about uncertainty under a Bayesian paradigm (Nixon et al. 2022, Gustafson 2015). Still, in some situations, it may be more appropriate to impose identification restrictions on the model, ignoring this source of uncertainty. Identifiability can be imposed through sum-to-zero constrains on each function  $\mathbf{f}^{(k)}$  (e.g.,  $\int \mathbf{f}^{(k)} d\mathbf{Z}^{(k)} = \mathbf{0}$ ) (Hastie 2017) or through modified kernel functions which impose identification (Lu et al. 2022). Both methods can be used with MultiAddGPs. For simplicity, this article uses an approximation of the sum-to-zero approach. Assuming the number of evaluation points  $N^*$  is sufficiently large and comes from a sufficiently diverse portion of the covariate space, the sum-to-zero constraint can be accurately approximated by centering posterior samples of each function via

$$\tilde{\mathbf{f}}^{(k)} = \mathbf{f}^{(k)}(z^{(k)}) - \frac{1}{n} \sum_{n=1}^N \mathbf{f}^{(k)}(z_n^{(k)}).$$

We find this method is computationally efficient, easy to implement, and provides similar results to alternative methods.

## 2.4 Inferring Model Hyperparameters

Hyperparameter selection remains an outstanding problem in MLTPs (Silverman et al. 2022). Here we demonstrate how the same Laplace approximation used in the Collapse step of the CU sampler can be used to approximate marginal likelihoods and thereby estimate hyperparameters via Maximum Marginal Likelihood (MML) or penalized MML estimation.

Let  $\Omega$  denote a set of hyperparameters in the joint MLTPs distribution:  $p(\mathbf{H}, \Phi, \mathbf{Y} \mid \Omega)$ . These can be parameters in a kernel, a mean function, or even in the log-ratio transformation  $\phi$ . The MML estimate for  $\Omega$  is

$$\hat{\Omega} = \operatorname{argmax}_{\Omega} \int p(\mathbf{H}, \Phi, \mathbf{Y} \mid \Omega) d\Phi d\mathbf{H} \quad (5)$$

This is equivalent to the MML estimate of the collapsed form since  $\int p(\mathbf{H}, \Phi, \mathbf{Y} \mid \Omega) d\Phi = p(\mathbf{H}, \mathbf{Y} \mid \Omega)$ . A first-order Laplace approximation to this integral is given by:

$$\log \int p(\mathbf{H}, \mathbf{Y} \mid \Omega) d\mathbf{H} \approx \frac{(D-1)N}{2} \log(2\pi) + \log p(\hat{\mathbf{H}}_{\Omega}, \mathbf{Y} \mid \Omega) - \frac{1}{2} \log(|\nabla^2[\operatorname{vec}(\hat{\mathbf{H}}_{\Omega})]|) \quad (6)$$

where  $\hat{\mathbf{H}}_{\Omega}$  denotes the MAP estimate for  $\mathbf{H}$  evaluated in the observed set  $\{1, \dots, N\}$  which depends on the hyperparameters  $\Omega$ . From a computational standpoint, this Laplace approximation to the marginal likelihood is essentially free given that we are already computing the MAP estimate and a factorization of the Hessian matrix during the CU sampler. Beyond MML estimation, it is simple to add additional penalization when defining weakly identified MultiAddGPs.

In practice, we estimate hyperparameters by maximizing Equation (6), either with or without additional penalization. While various optimization routines can be used to perform the optimization, the problem is often non-convex, especially when estimating

bandwidth parameters in kernel functions. For this reason, we generally recommend Bayesian optimization procedures, which can optimize non-convex functions while simultaneously reducing the number of function evaluations compared to more typical optimizers (e.g., the L-BFGS optimizer). We have tested and found Bayesian optimization procedures generally work well when  $\Omega$  is of low to moderate dimension (e.g.,  $\leq 10$ ). When  $\Omega$  is higher dimensional, alternative procedures may be needed. In this study, Bayesian Optimization was performed using the *ParBayesianOptimization* R package with the acquisition function set to the upper confidence bound, starting with 10 initial points and proceeding through 20 iterations with all other parameters set to their default values.

## 2.5 Software Availability

We have made MultiAddGPs available through the R package *fido* (Silverman & Nixon 2021), where it can be accessed via the `basset` function. The *fido* package implements the extended CU sampler described above using optimized C++ code. MAP estimation of  $\hat{H}$  is performed using the L-BFGS optimizer. Hyperparameter selection by MML is performed by maximizing the marginal likelihood using Bayesian optimization implemented in the *ParBayesianOptimization* R package (Wilson 2022). All code required to reproduce the results of this article is available at <https://github.com/Silverman-Lab/MultiAddGPs>.

## 3 Simulations

To evaluate the performance of the proposed model relative to existing methods, we conduct two simulation studies. The first study highlights the importance of accounting for uncertainty introduced by the measurement process, which is ignored by LongGP (Cheng et al. 2019). The second study compares the performance of MultiAddGPs to Lgpr (Timonen et al. 2021). However, due to the high computational cost of Lgpr, we were unable to scale

it to the full simulation setting. Instead, we perform a smaller-scale simulation to compare MultiAddGPs and Lgpr. Full simulation details are provided in Supplementary Section 5.

### 3.1 Simulation 1

We simulated longitudinal microbiome studies with varying numbers of taxa  $D \in \{3, \dots, 100\}$  and samples  $N \in \{50, \dots, 1000\}$ . We simulated microbial composition influenced by batch effects, daily periodicity (e.g., circadian rhythm; Heddes et al. (2022)), and longer-term trends. For this simulation study we did not compare to Lgpr or LongGP for two reasons: (1) it was too computationally intensive and could not scale to the larger simulation sizes; (2) it could not model periodic components as it lacked periodic kernels. Instead, we created a new method *Normal Additive GPs (NAddGPs)* which assumes the data are transformed Gaussian and are therefore reminiscent of LongGP. NAddGPs are nearly identical to MultiAddGPs but assume each  $\mathbf{H}_n$  is observed and equal to  $\mathbf{H}_n = \phi(\mathbf{Y}_n + 0.5 \cdot \mathbf{1}_D)$  and therefore proceed directly to the uncollapse step, skipping the collapsed step of our CU sampler.

In Figure 1 we show a small simulation  $D = 4$  and  $N = 600$  for ease of visualization. We use  $t_n$  to denote the time at which sample  $n$  was obtained. For inference, we specified MultiAddGPs and NAddGPs models as  $\mathbf{F}_n = \mathbf{b}_0 + \mathbf{b}_1 x_n^{(\text{batch})} + \mathbf{f}^{(\text{periodic})}(t_n) + \mathbf{f}^{(\text{trend})}(t_n)$ . For covariates, we set  $\mathbf{X}_n = [1 x_n^{(\text{batch})}]^T$ ,  $\mathbf{Z}_n^{(\text{periodic})} = t_n$ , and  $\mathbf{Z}_n^{(\text{trend})} = t_n$ . For priors we set  $\mathbf{B} = [\mathbf{b}_0 = 2.7; \mathbf{b}_1 = 1]$ . Both  $\mathbf{f}^{(\text{periodic})}$  and  $\mathbf{f}^{(\text{trend})}$  were given matrix-normal process priors with mean function  $\Theta^{(k)} = \mathbf{0}$ . A periodic kernel  $K_{\text{period}}(t, t') = \sigma_{\text{period}} \exp\left(-\frac{1}{\rho_{\text{period}}^2} 2 \sin^2\left(\frac{\pi|t-t'|}{p}\right)\right)$  was used in the prior for  $\mathbf{f}^{(\text{periodic})}$  and a squared exponential  $K_{\text{trend}}(t, t') = \sigma_{\text{trend}}^2 \exp\left(-\frac{1}{2\rho_{\text{trend}}^2}(t-t')^2\right)$  was used for  $\mathbf{f}^{(\text{trend})}$ . Hyperparameters  $\Omega = \{\sigma_{\text{period}}, \rho_{\text{period}}, p, \sigma_{\text{trend}}, \rho_{\text{trend}}\}$  were selected using MML estimation.

We compared posterior estimates from the MultiAddGPs and NAddGPs models to em-

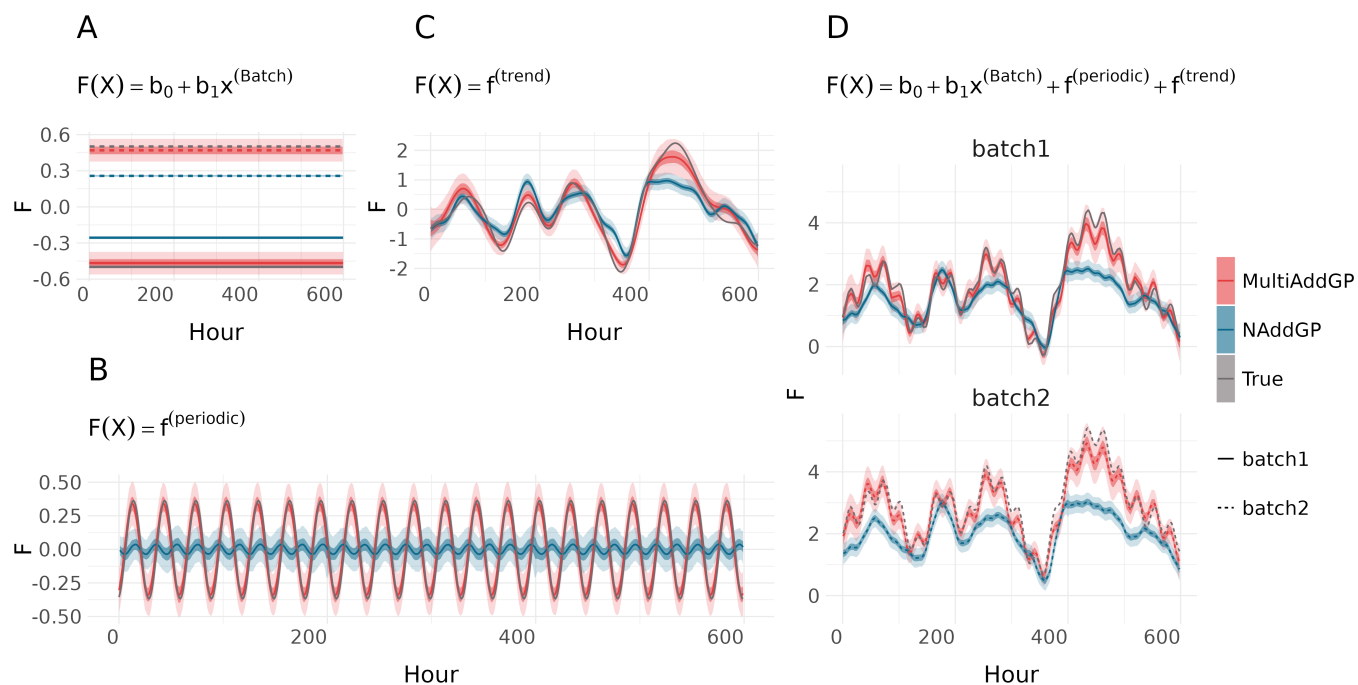


Figure 1: **MultiAddGPs successfully decompose simulated microbiome time-series.** The NAddGPs model is identical to the MultiAddGPs model but ignores uncertainty due to counting by modeling the observed data as transformed Gaussian. Panels A, B, and C represent individual decomposed components associated with each covariate. Panel D illustrates the cumulative effect of all components. In all panels, MultiAddGPs more accurately recover the true underlying signal compared to NAddGPs.

phasize the importance of modeling uncertainty due to counting. Figure 1 shows that the MultiAddGPs almost perfectly recovered the true decomposition whereas the NAddGPs substantially underestimated the amplitude of the periodic component and long-term trend. Figure 2 shows these findings generalize as  $N$  and  $D$  increase. As the posterior of these high-dimensional models cannot be easily visualized, we quantified model performance based on the coverage of posterior 95% intervals with respect to the true function decomposition. Since both MultiAddGPs and NAddGPs are Bayesian models, we do not expect that these intervals will cover the truth with 95% probability. As a result, we focus on the ratio of

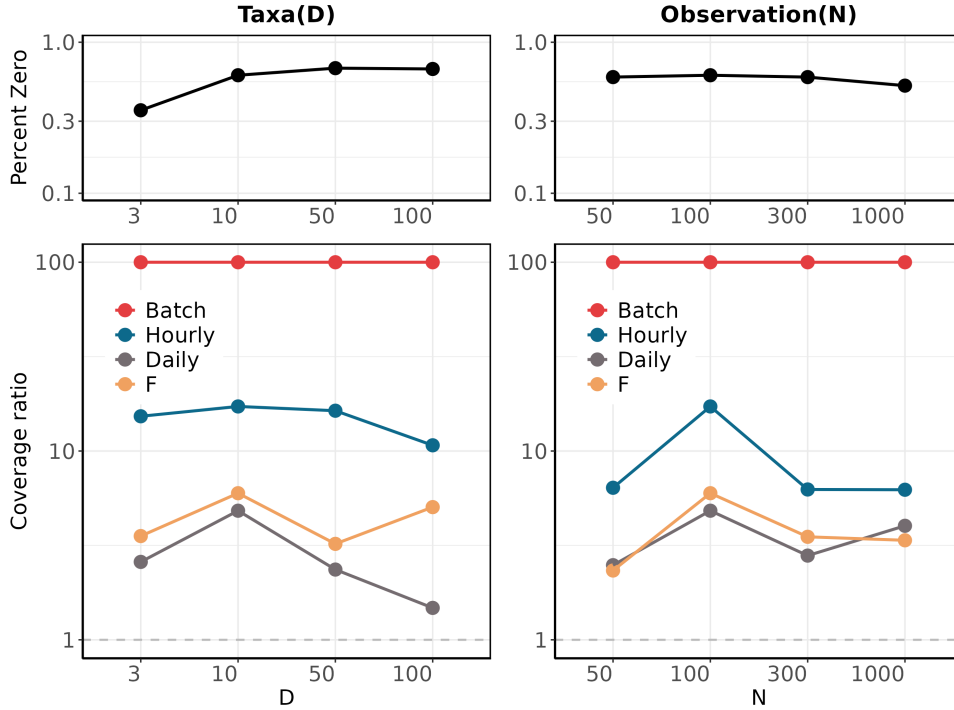


Figure 2: **At all tested dimensions  $N$  and  $D$ , posterior intervals from MultiAddGPs cover the truth more frequently than NAddGPs.** The first row illustrates how data sparsity varied with dimensions  $N$  and  $D$  in our simulation studies. The second row shows the ratio between coverage of 95% Credible intervals from MultiAddGPs compared to NAddGPs. Each datapoint represents the mean over three simulations. The ratio is always positive, illustrating that MultiAddGPs cover the truth substantially more than NAddGPs. Coverage ratios for each of the decomposed components *Batch*, *Hourly*, and *Daily* and the cumulative function  $\mathbf{F}$  are shown.

coverage between the MultiAddGPs and the NAddGPs. Positive values of this coverage ratio indicate that the MultiAddGPs model covers the truth more often than the NAddGPs model. In all simulations, at all sample sizes  $N$  and number of taxa  $D$ , the MultiAddGPs models covered the truth far more frequently than the NAddGPs models.

## 3.2 Simulation 2

To compare with Lgpr, which allows for negative binomial likelihoods, we conducted a smaller simulation with  $D = 3$  taxa and  $N = 50$  samples. Since Lgpr employs predefined kernel structures and does not incorporate a periodic kernel, we designed the simulation based on an alternative latent function  $\mathbf{F}_n = \mathbf{b}_0 + \mathbf{b}_1 x_n^{(\text{batch})} + \mathbf{f}^{(\text{non-stationary})}(t_n) + \mathbf{f}^{(\text{trend})}(t_n)$ . We chose priors for Lgpr that matched the priors used for our MultiAddGPs.

Lgpr required approximately seven hours to analyze a single taxon on a high-performance computing cluster, resulting in an effective sample size of only 100 (Gelman et al. 2015). In contrast, MultiAddGPs simultaneously analyzed all taxa in about one minute and produced an effective sample size of 2000. In summary, our method produces effective samples at over 240,000 times the rate of Lgpr.

Our methods not only demonstrate increased efficiency, but the posterior estimates obtained using MultiAddGPs also align more closely with the true function decomposition compared to those derived from Lgpr (see Supplementary Figure 3).

## 4 Application to Artificial Human Guts

We used MultiAddGPs to reanalyze a previously published longitudinal study of four artificial gut models (Silverman et al. 2018). This study consists of over 500 samples from 4 artificial gut vessels irregularly spaced through time. The key feature of this study was the starvation of Vessels 1 and 2 that occurred over days 11 to 13 while Vessels 3 and 4 received no intervention and therefore act as controls. The study were previously be analyzed by Silverman et al. (2022) and Silverman et al. (2018), who show that microbiota demonstrate a prolonged recovery phase after feeding resumes. However, previous models could not disentangle long-term temporal trends from the specific effects of starvation, leaving the

dynamics of the recovery phase poorly understood. We use a MultiAddGPs model to overcome this limitation and provide novel insights into these microbial communities.

Data preprocessing followed the analysis of [Silverman et al. \(2018\)](#) and resulted in 10 bacterial families and 537 samples. We modeled these data as consisting of two overlapping temporal processes, a vessel-specific long-term trend  $f^{(\text{base},v)}$  and a vessel-specific function representing the effect of starvation  $f^{(\text{disrupt},v)}$ . We used the following MultiAddGPs model:

$$\begin{aligned}
\mathbf{Y}_{\cdot n} &\sim \text{Multinomial}(\mathbf{\Pi}_{\cdot n}) \\
\mathbf{\Pi}_{\cdot n} &= \text{ALR}_D^{-1}(\mathbf{H}_{\cdot n}) \\
\mathbf{H}_{\cdot n} &\sim N(\mathbf{F}_{\cdot n}, \mathbf{\Sigma}) \\
\mathbf{F} &= \sum_{v=1}^4 (\mathbf{f}^{(\text{base},v)}(t_n) + I[v \in \{1, 2\}] \mathbf{f}^{(\text{disrupt},v)}(t)) \\
\mathbf{f}^{(\text{base},v)} &\sim \text{GP}(\mathbf{\Theta}^{(\text{base},v)}, \mathbf{\Sigma}, \mathbf{\Gamma}^{(v)} \odot \mathbf{\Gamma}^{(\text{base})}), v \in \{1, 2, 3, 4\} \\
\mathbf{f}^{(\text{disrupt},v)} &\sim \text{GP}(\mathbf{\Theta}^{(\text{disrupt},v)}, \mathbf{\Sigma}, \mathbf{\Gamma}^{(v)} \odot \mathbf{\Gamma}^{(\text{disrupt})}), v \in \{1, 2\} \\
\mathbf{\Sigma} &\sim \text{InvWishart}(\mathbf{\Xi}, \zeta)
\end{aligned}$$

where  $\mathbf{\Xi}$  was chosen following [Silverman et al. \(2022\)](#) to reflect the phylogenetic relationships between taxa.  $\zeta = D+5$  was chosen to reflect weak prior knowledge of the importance of these relationships. Within the kernel functions,  $\odot$  represents elementwise multiplication of kernels. The kernel  $\mathbf{\Gamma}^{(v)}$  was block diagonal with all non-zero elements equal to 1: it was used to model conditional independence between the vessels.  $\mathbf{\Gamma}^{(\text{base})}$  was modeled as a squared exponential kernel to capture long-term non-linear trends. In contrast,  $\mathbf{\Gamma}^{(\text{disrupt})}$  was modeled using a rational quadratic kernel, which was forced to zero before day 11 to reflect our knowledge that starvation started on day 11. Hyperparameters  $\Omega = \{\sigma_{\text{base}}, \rho_{\text{base}}, \sigma_{\text{disrupt}}, \rho_{\text{disrupt}}\}$  were selected using penalized MML. Full details on penalization, kernel, and mean functions are provided in Supplementary Section 6.

Posterior estimates for the cumulative function  $F$  (long-term trend plus starvation effect)

are shown in Figure 3. Posterior estimates for the decomposed starvation effect are shown in Figure 4. Consistent with prior reports, the *Rikenellaceae* family demonstrates a substantial decrease during the initial starvation period, followed by a slow recovery to baseline (Silverman et al. 2018, Sun & Zhou 2024). This finding is notable given that decreases in *Rikenellaceae* are also observed in obese individuals (Okeke et al. 2014, Peters et al. 2018, Tavella et al. 2021). As obesity and starvation seem like opposite conditions, decreased *Rikenellaceae* relative abundance in both conditions suggests that host factors not present in these artificial gut systems but present in *in vivo* obesity studies (e.g., the host immune system) may be driving the decreases in obesity.

Our MultiAddGPs also reveal new features of this data and suggest novel biology. For example, our model finds strong evidence that the *Rikenellaceae* relative abundance in the community decreases drastically during the initial starvation event, followed by a later over-correction where their abundance ultimately increases before trending back to pre-starvation levels. These types of over-corrections are predicted by ecological predator-prey models, which can lead to damped oscillations in response to exogenous stimuli (Samuelson 1971). To best of our knowledge, this is the first study to demonstrate phenomena consistent with that theory within *in vitro* systems.

## 5 Application to Longitudinal Microbiome Data

We reanalyzed a human gut microbiome study wherein the study participant collected daily fecal samples over the course of one year (David, Materna, Friedman, Campos-Baptista, Blackburn, Perrotta, Erdman & Alm 2014). While the original dataset had samples from two donors, we focus on the gut microbiome data from Subject A, as this subject demonstrated a substantial shift in community composition during a period of prolonged international travel (David, Materna, Friedman, Campos-Baptista, Blackburn, Perrotta, Erdman &

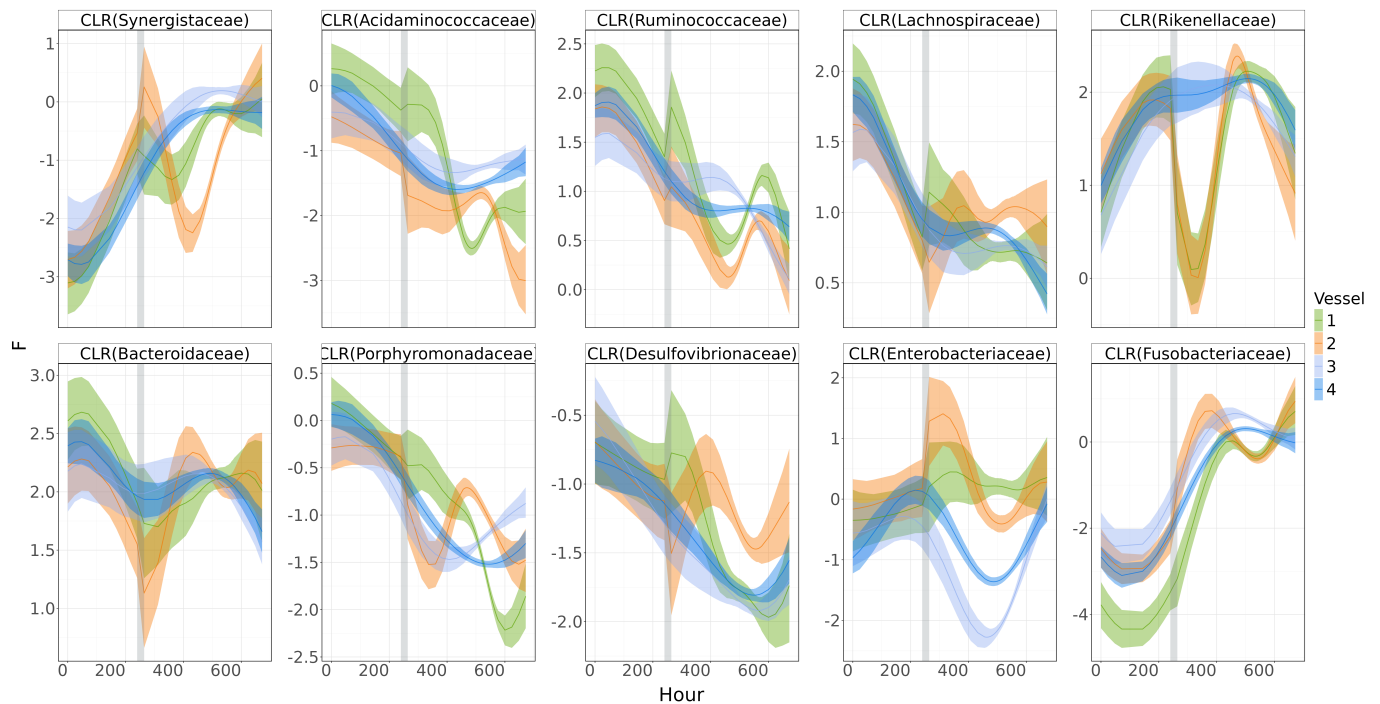


Figure 3: **MultiAddGPs Posterior for the Smoothed State  $\mathbf{F}$  of an Artificial Gut Study.** As described in the main text,  $\mathbf{F}$  was modeled as the additive combination of a slowly-varying temporal trend and a more variable yet short-lived starvation effect in Vessels 1 and 2 which started on Day 11. Posterior mean and 95% credible intervals of  $\mathbf{F}$  are shown for each of the four artificial gut vessels. We plot these results with respect to the Centered Log-Ratio (CLR) Coordinates of each bacterial family. The starvation event, which occurred between Days 11 and 13 in Vessels 1 and 2, is highlighted in Gray.

Alm 2014). While this study has been analyzed by multiple authors (Gibbons et al. 2017, Duvallet et al. 2017), we are the first to produce direct estimates of the effect of travel, partitioning those effects from background temporal variation (see Figure 5).

Data was obtained from European Bioinformatics Institute (EBI) with accession number SAMEG179160 and processed following the methods of David, Materna, Friedman, Campos-Baptista, Blackburn, Perrotta, Erdman & Alm (2014), with the exception that we used DADA2 (Callahan et al. 2016) to call sequence variants rather than the OTU calling methods

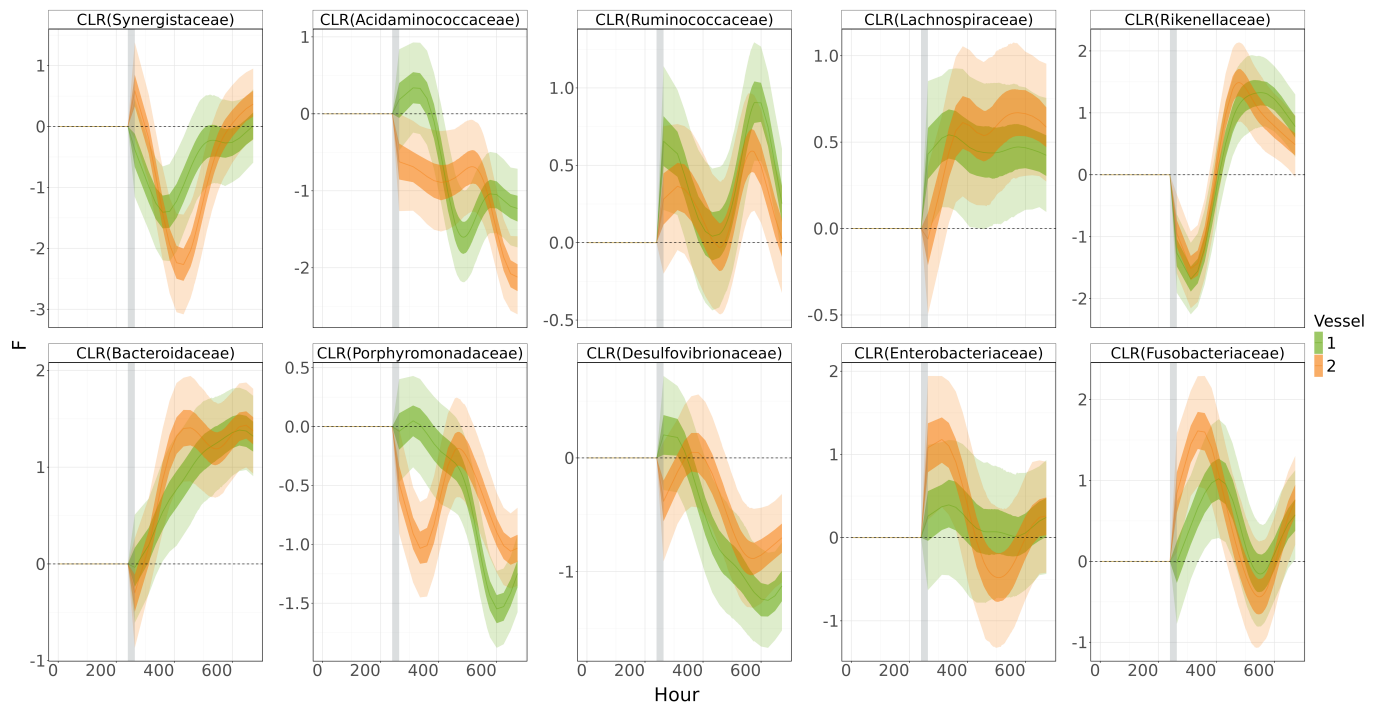


Figure 4: **MultiAddGPs Posterior for the Starvation effect ( $f^{(\text{disrupt})}$ ) in Artificial Gut Study.** Posterior mean, 50% and 95% credible intervals are shown for all taxa.

used in the original study. In total, we analyzed 47 bacterial families over 263 time-points. We modeled these data as consisting of two overlapping temporal components: a long-term trend, denoted as  $f^{(\text{trend})}$ , and a non-stationary function representing the effect of travel intervention, denoted as  $f^{(\text{travel})}$ . The data were analyzed using the following MultiAddGPs

model:

$$\begin{aligned}
\mathbf{Y}_{\cdot n} &\sim \text{Multinomial}(\mathbf{\Pi}_{\cdot n}) \\
\mathbf{\Pi}_{\cdot n} &= \text{ALR}_D^{-1}(\mathbf{H}_{\cdot n}) \\
\mathbf{H}_{\cdot n} &\sim N(\mathbf{F}_{\cdot n}, \mathbf{\Sigma}) \\
\mathbf{F} &= \beta_0 + \mathbf{f}^{(\text{trend})}(t_n) + \mathbf{f}^{(\text{travel})}(t_n) \\
\mathbf{f}^{(\text{trend})} &\sim \text{GP}(\mathbf{\Theta}^{(\text{trend})}, \mathbf{\Sigma}, \mathbf{\Gamma}^{(\text{trend})}) \\
\mathbf{f}^{(\text{travel})} &\sim \text{GP}(\mathbf{\Theta}^{(\text{travel}, v)}, \mathbf{\Sigma}, \mathbf{\Gamma}^{(\text{travel})}) \\
\mathbf{\Sigma} &\sim \text{InvWishart}(\mathbf{\Xi}, \zeta)
\end{aligned}$$

where  $\mathbf{\Xi}$  was chosen following [Silverman et al. \(2022\)](#) to reflect the phylogenetic relationships between taxa.  $\zeta = D + 100$  was chosen to reflect moderately strong prior knowledge of the importance of these relationships. A squared exponential kernel ( $\mathbf{\Gamma}^{\text{trend}}$ ) was used to capture long-term nonlinear trends, while a non-stationary kernel with a non-linear warp function ( $\mathbf{\Gamma}^{\text{travel}}$ ) used to capture the shorter-term non-linear effect of travel. Hyperparameters  $\Omega = \{\sigma_{\text{trend}}, \rho_{\text{trend}}, \sigma_{\text{travel}}, \rho_{\text{travel}}\}$  were estimated using penalized MML. [Figure 5](#) shows the contribution of each component and the cumulative effects. Consistent with [David, Maurice, Carmody, Gootenberg, Button, Wolfe, Ling, Devlin, Varma, Fischbach et al. \(2014\)](#), our findings indicate that while the microbiome remains relatively stable over the long term, travel events induce significant perturbations in community composition. Full details of the analysis are provided in [Supplementary Section 7](#).

## 6 Discussion

Motivated by applied statistical challenges in the analysis of microbiota data, we have introduced a class of Bayesian Multinomial Logistic-Normal additive linear and non-linear regression models (MultiAddGPs). Using recent theory on Marginally Latent Matrix-t

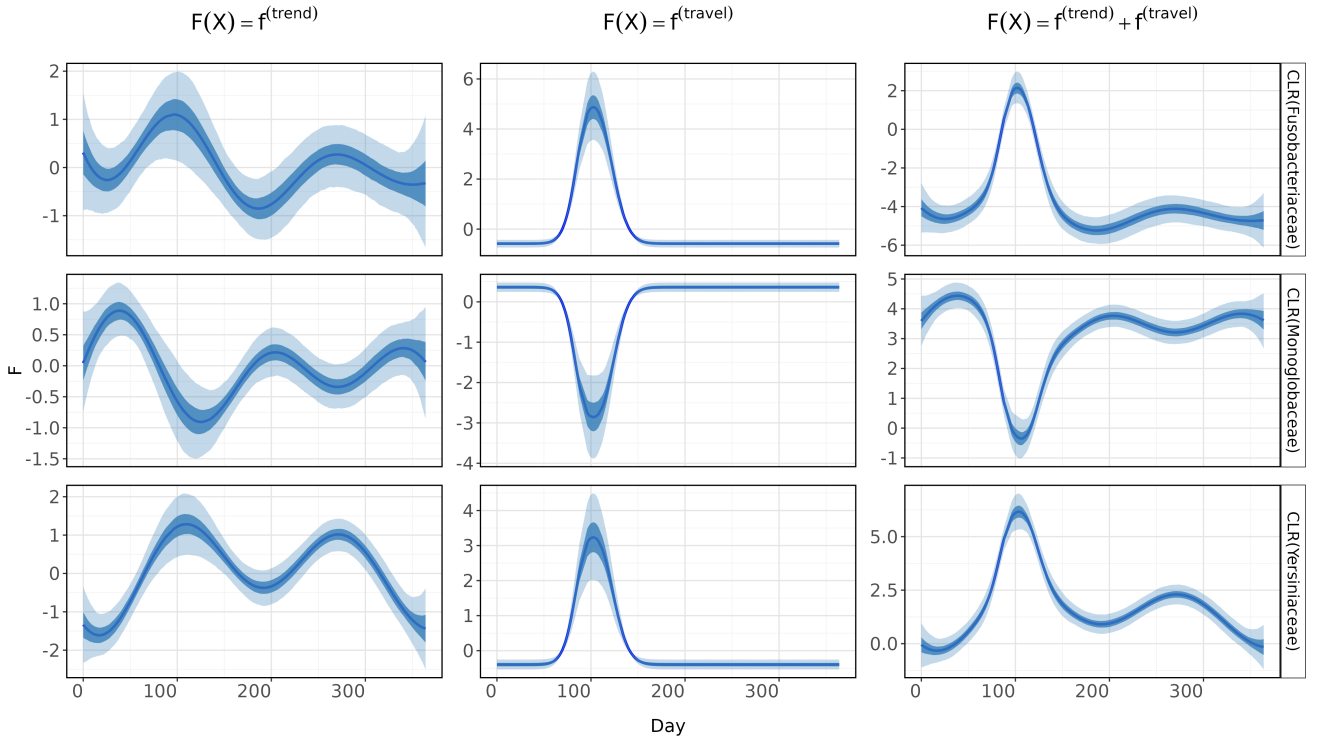


Figure 5: **Posterior of each component and their cumulative effect for bacterial families *Fusobacteriaceae*, *Monoglobaceae*, and *Yersiniaceae* (Longitudinal microbiome data).** Each row shows contribution of individual components ( $\mathbf{f}^{(\text{trend})}$  and  $\mathbf{f}^{(\text{travel})}$ ) and the final column presents the cumulative effect ( $\mathbf{f}^{(\text{trend})} + \mathbf{f}^{(\text{travel})}$ ). Results are reported in terms of Centered Log-Ratio (CLR) coordinates, along with posterior means and corresponding 50% as well as 95% credible intervals.

Processes (MLTPs), we have developed efficient inference and hyperparameter estimation algorithms for this class of models. Additionally, we have incorporated non-stationary kernel functions designed to model treatment interventions and disease effects, allowing capture of complex microbiome dynamics. Beyond MultiAddGPs, our hyperparameter estimation techniques can be applied in the much larger class of MLTPs that can be sampled using the CU Sampler. Our methods have been made widely available as part of the *fido* R package, which is published on CRAN.

While our methods are inspired by challenges in microbiome data, MultiAddGPs could be applied broadly to other settings where count compositional data is collected, including gene expression studies (Fernandes et al. 2014), macro-ecology (Billheimer et al. 2001), and even political polling (Topîrceanu & Precup 2020). Still, key challenges and future directions remain.

This article develops an efficient approach to hyperparameter selection via approximate MML and penalized MML estimation. An advantage of our approach is its flexibility: researchers can optimize hyperparameters within a kernel function or even within the log-ratio transformation. In practice, we have found Bayesian Optimization to be a practical approach to maximizing the approximate marginal likelihood with small to moderate numbers of hyperparameters (e.g.,  $<10$ ). Further research and improvement are likely needed when selecting larger numbers of hyperparameters simultaneously or when the optimization landscape is particularly challenging.

Besides the challenge of calculating MML and penalized MML estimates, alternative methods of selecting hyperparameters may be needed. In particular, some researchers may require fully Bayesian solutions that can quantify uncertainty in model hyperparameters. This is the notable advantage of Cheng et al. (2019) approach. While their model ignores counting variation, and assumes the data is transformed Gaussian, their method provides fully Bayesian inference of hyperparameters via the slice sampler of Murray & Adams (2010). We expect that the same slice-sampling approach could be used for MultiAddGPs, replacing the Metropolis-Hastings Steps used in that method with the CU sampler with marginal Laplace approximation.

Finally, readers should be aware of the limits of the Laplace Approximation in the CU sampler when inferring Multinomial Logistic-Normal MLTPs. In Silverman et al. (2022), we proved that the error rate of this Laplace approximation is of order  $O_p([D - 1] \sum_{n=1}^N [\sum_{d=1}^D Y_{dn}]^{-1})$ .

This result implies that the approximation works well when the average number of counts per sample (e.g., the sequencing depth) is high. This is the case with modern sequencing technologies. In contrast, we expect the approximation will be poor when there are few counts per sample, for example, when observations are categorical ( $\sum_{d=1}^D Y_{dn} = 1$ ). In this scenario, alternative methods, such as the Debiased Multinomial Dirichlet Bootstrap from [Saxena et al. \(2024\)](#), may be necessary.

## 7 Disclosure statement

The authors have the following conflicts of interest to declare.

## 8 Data Availability Statement

All data and code needed to reproduce the analyses in this article are available at <https://github.com/Silverman-Lab/MultiAddGPs>.

### SUPPLEMENTAL MATERIALS

**Supplement** includes the following parts: a review of the Collapse-Uncollapsed (CU) sampler and Laplace Approximation in the Collapsed step, a derivation of the posterior distribution for the matrix conjugate linear model, a theoretical result on MLTP for MultiAddGP models, and additional simulation and application details.

## References

- Äijö, T., Müller, C. L. & Bonneau, R. (2018), ‘Temporal probabilistic modeling of bacterial compositions derived from 16S rRNA sequencing’, *Bioinformatics* **34**(3), 372–380.
- Aitchison, J. & Shen, S. M. (1980), ‘Logistic-normal distributions - some properties and

uses', *Biometrika* **67**(2), 261–272.

**URL:** <Go to ISI>://WOS:A1980KA99800001

Ballen, K., Ahn, K. W., Chen, M., Abdel-Azim, H., Ahmed, I., Aljurf, M., Antin, J., Bhatt, A. S., Boeckh, M., Chen, G. et al. (2016), 'Infection rates among acute leukemia patients receiving alternative donor hematopoietic cell transplantation', *Biology of blood and marrow transplantation* **22**(9), 1636–1645.

Billheimer, D., Guttorp, P. & Fagan, W. F. (2001), 'Statistical interpretation of species composition', *Journal of the American statistical Association* **96**(456), 1205–1214.

Callahan, B. J., McMurdie, P. J., Rosen, M. J., Han, A. W., Johnson, A. J. A. & Holmes, S. P. (2016), 'Dada2: High-resolution sample inference from illumina amplicon data', *Nature Methods* **13**(7), 581–583.

Cheng, L., Ramchandran, S., Vatanen, T., Lietzen, N., Lahesmaa, R., Vehtari, A. & Lahdesmaki, H. (2019), 'An additive Gaussian process regression model for interpretable non-parametric analysis of longitudinal data', *Nature Communications* **10**(1), 1798.

**URL:** <https://www.nature.com/articles/s41467-019-09785-8>

David, L. A., Materna, A. C., Friedman, J., Campos-Baptista, M. I., Blackburn, M. C., Perrotta, A., Erdman, S. E. & Alm, E. J. (2014), 'Host lifestyle affects human microbiota on daily timescales', *Genome Biology* **15**, 1–15.

David, L. A., Maurice, C. F., Carmody, R. N., Gootenberg, D. B., Button, J. E., Wolfe, B. E., Ling, A. V., Devlin, A. S., Varma, Y., Fischbach, M. A. et al. (2014), 'Diet rapidly and reproducibly alters the human gut microbiome', *Nature* **505**(7484), 559–563.

Duvallet, C., Gibbons, S. M., Gurry, T., Irizarry, R. A. & Alm, E. J. (2017), 'Meta-analysis of gut microbiome studies identifies disease-specific and shared responses', *Nature Communications* **8**(1), 1784.

- Fernandes, A. D., Reid, J. N., Macklaim, J. M., McMurrough, T. A., Edgell, D. R. & Gloor, G. B. (2014), ‘Unifying the analysis of high-throughput sequencing datasets: characterizing rna-seq, 16s rrna gene sequencing and selective growth experiments by compositional data analysis’, *Microbiome* **2**, 1–13.
- Fрати, F., Salvatori, C., Incorvaia, C., Bellucci, A., Di Cara, G., Marcucci, F. & Esposito, S. (2018), ‘The role of the microbiome in asthma: the gut–lung axis’, *International Journal of Molecular Sciences* **20**(1), 123.
- Gao, M., Xiong, C., Gao, C., Tsui, C. K., Wang, M.-M., Zhou, X., Zhang, A.-M. & Cai, L. (2021), ‘Disease-induced changes in plant microbiome assembly and functional adaptation’, *Microbiome* **9**, 1–18.
- Gelman, A., Lee, D. & Guo, J. (2015), ‘Stan: A probabilistic programming language for bayesian inference and optimization’, *Journal of Educational and Behavioral Statistics* **40**(5), 530–543.
- Gibbons, S. M., Kearney, S. M., Smillie, C. S. & Alm, E. J. (2017), ‘Two dynamic regimes in the human gut microbiome’, *PLoS Computational Biology* **13**(2), e1005364.
- Glassner, K. L., Abraham, B. P. & Quigley, E. M. (2020), ‘The microbiome and inflammatory bowel disease’, *Journal of Allergy and Clinical Immunology* **145**(1), 16–27.
- Gloor, G. B., Macklaim, J. M., Pawlowsky-Glahn, V. & Egozcue, J. J. (2017), ‘Microbiome datasets are compositional: and this is not optional’, *Frontiers in Microbiology* **8**, 2224.
- Gloor, G. B., Macklaim, J. M., Vu, M. & Fernandes, A. D. (2016), ‘Compositional uncertainty should not be ignored in high-throughput sequencing data analysis’, *Austrian Journal of Statistics* **45**(4), 73–87.

- Grantham, N. S., Guan, Y., Reich, B. J., Borer, E. T. & Gross, K. (2020), ‘Mimix: A bayesian mixed-effects model for microbiome data from designed experiments’, *Journal of the American Statistical Association* **115**(530), 599–609.
- Gustafson, P. (2015), *Bayesian inference for partially identified models: Exploring the limits of limited data*, Vol. 140, CRC Press.
- Hastie, T. J. (2017), Generalized additive models, in ‘Statistical models in S’, Routledge, pp. 249–307.
- Heddes, M., Altaha, B., Niu, Y., Reitmeier, S., Kleigrewe, K., Haller, D. & Kiessling, S. (2022), ‘The intestinal clock drives the microbiome to maintain gastrointestinal homeostasis’, *Nature Communications* **13**(1), 6068.
- Helmink, B. A., Khan, M. W., Hermann, A., Gopalakrishnan, V. & Wargo, J. A. (2019), ‘The microbiome, cancer, and cancer therapy’, *Nature Medicine* **25**(3), 377–388.
- Holleran, G., Scaldaferri, F., Ianiro, G., Lopetuso, L., Mc Namara, D., Mele, M. C., Gasbarrini, A. & Cammarota, G. (2018), ‘Fecal microbiota transplantation for the treatment of patients with ulcerative colitis and other gastrointestinal conditions beyond clostridium difficile infection: an update.’, *Drugs of Today (Barcelona, Spain: 1998)* **54**(2), 123–136.
- Honda, K. & Littman, D. R. (2012), ‘The microbiome in infectious disease and inflammation’, *Annual Review of Immunology* **30**(1), 759–795.
- Kaul, A., Mandal, S., Davidov, O. & Peddada, S. D. (2017), ‘Analysis of microbiome data in the presence of excess zeros’, *Frontiers in Microbiology* **8**, 2114.
- Kostic, A. D., Xavier, R. J. & Gevers, D. (2014), ‘The microbiome in inflammatory bowel disease: current status and the future ahead’, *Gastroenterology* **146**(6), 1489–1499.

- Kuczynski, J., Lauber, C. L., Walters, W. A., Parfrey, L. W., Clemente, J. C., Gevers, D. & Knight, R. (2012), ‘Experimental and analytical tools for studying the human microbiome’, *Nature Reviews Genetics* **13**(1), 47–58.
- Ley, R. E. (2010), ‘Obesity and the human microbiome’, *Current Opinion in Gastroenterology* **26**(1), 5–11.
- Li, H. (2015), ‘Microbiome, metagenomics, and high-dimensional compositional data analysis’, *Annual Review of Statistics and Its Application* **2**, 73–94.
- Lu, X., Boukouvalas, A. & Hensman, J. (2022), Additive gaussian processes revisited, in ‘International Conference on Machine Learning’, PMLR, pp. 14358–14383.
- Mao, J. & Ma, L. (2022), ‘Dirichlet-tree multinomial mixtures for clustering microbiome compositions’, *The Annals of Applied Statistics* **16**(3), 1476.
- McGregor, K., Okaeme, N., Khorasaniha, R., Veniamin, S., Jovel, J., Miller, R., Mahmood, R., Graham, M., Bonner, C., Bernstein, C. N. et al. (2023), ‘Proportionality-based association metrics in count compositional data’, *bioRxiv* pp. 2023–08.
- Murray, I. & Adams, R. P. (2010), ‘Slice sampling covariance hyperparameters of latent Gaussian models’, *Advances in neural information processing systems* **23**.
- Nixon, M. P., McGovern, K. C., Letourneau, J., David, L. A., Lazar, N. A., Mukherjee, S. & Silverman, J. D. (2022), ‘Scale reliant inference’, *arXiv preprint arXiv:2201.03616* .
- Okeke, F., Roland, B. C. & Mullin, G. E. (2014), ‘The role of the gut microbiome in the pathogenesis and treatment of obesity’, *Global advances in health and medicine* **3**(3), 44–57.
- Pawlowsky-Glahn, V., Egozcue, J. J. & Tolosana-Delgado, R. (2015), *Modeling and Analysis of Compositional Data*, John Wiley & Sons.

- Peters, B. A., Shapiro, J. A., Church, T. R., Miller, G., Trinh-Shevrin, C., Yuen, E., Friedlander, C., Hayes, R. B. & Ahn, J. (2018), ‘A taxonomic signature of obesity in a large study of american adults’, *Scientific Reports* **8**(1), 9749.
- Samuelson, P. A. (1971), ‘Generalized predator-prey oscillations in ecological and economic equilibrium’, *Proceedings of the National Academy of Sciences* **68**(5), 980–983.
- Sankaran, K. & Jeganathan, P. (2024), ‘mbtransfer: Microbiome intervention analysis using transfer functions and mirror statistics’, *PLOS Computational Biology* **20**(6), e1012196.
- Saxena, M., Chen, T. & Silverman, J. D. (2024), ‘Scalable inference for bayesian multinomial logistic-normal dynamic linear models’, *arXiv preprint arXiv:2410.05548* .
- Schwabe, R. F. & Jobin, C. (2013), ‘The microbiome and cancer’, *Nature Reviews Cancer* **13**(11), 800–812.
- Schwager, E., Mallick, H., Vents, S. & Huttenhower, C. (2017), ‘A bayesian method for detecting pairwise associations in compositional data’, *PLoS Computational Biology* **13**(11), e1005852.
- Sharon, G., Cruz, N. J., Kang, D.-W., Gandal, M. J., Wang, B., Kim, Y.-M., Zink, E. M., Casey, C. P., Taylor, B. C., Lane, C. J. et al. (2019), ‘Human gut microbiota from autism spectrum disorder promote behavioral symptoms in mice’, *Cell* **177**(6), 1600–1618.
- Silverman, J. D., Bloom, R. J., Jiang, S., Durand, H. K., Dallow, E., Mukherjee, S. & David, L. A. (2021), ‘Measuring and mitigating pcr bias in microbiota datasets’, *PLoS Computational Biology* **17**(7), e1009113.
- Silverman, J. D., Durand, H. K., Bloom, R. J., Mukherjee, S. & David, L. A. (2018), ‘Dynamic linear models guide design and analysis of microbiota studies within artificial human guts’, *Microbiome* **6**(1), 1–20.

- Silverman, J. D. & Nixon, M. (2021), ‘FIDO: multinomial logistic-normal models’, *CRAN*.
- Silverman, J. D., Roche, K., Holmes, Z. C., David, L. A. & Mukherjee, S. (2022), ‘Bayesian multinomial logistic normal models through marginally latent matrix-t processes’, *The Journal of Machine Learning Research* **23**(1), 255–296.
- Silverman, J. D., Roche, K., Mukherjee, S. & David, L. A. (2020), ‘Naught all zeros in sequence count data are the same’, *Computational and Structural Biotechnology Journal* **18**, 2789–2798.
- Silverman, J. D., Washburne, A. D., Mukherjee, S. & David, L. A. (2017), ‘A phylogenetic transform enhances analysis of compositional microbiota data’, *eLife* **6**, e21887.
- Sun, G. & Zhou, Y.-H. (2024), ‘Predicting microbiome growth dynamics under environmental perturbations’, *Applied Microbiology* **4**(2), 948–958.
- Tavella, T., Rampelli, S., Guidarelli, G., Bazzocchi, A., Gasperini, C., Pujos-Guillot, E., Comte, B., Barone, M., Biagi, E., Candela, M. et al. (2021), ‘Elevated gut microbiome abundance of christensenellaceae, porphyromonadaceae and rikenellaceae is associated with reduced visceral adipose tissue and healthier metabolic profile in italian elderly’, *Gut Microbes* **13**(1), 1880221.
- Tilg, H., Kaser, A. et al. (2011), ‘Gut microbiome, obesity, and metabolic dysfunction’, *The Journal of Clinical Investigation* **121**(6), 2126–2132.
- Timonen, J., Mannerström, H., Vehtari, A. & Lähdesmäki, H. (2021), ‘lgpr: an interpretable non-parametric method for inferring covariate effects from longitudinal data’, *Bioinformatics* **37**(13), 1860–1867.
- Topîrceanu, A. & Precup, R.-E. (2020), ‘A framework for improving electoral forecasting based on time-aware polling’, *Social Network Analysis and Mining* **10**(1), 39.

- Vandeputte, D., Kathagen, G., D'hoë, K., Vieira-Silva, S., Valles-Colomer, M., Sabino, J., Wang, J., Tito, R. Y., De Commer, L., Darzi, Y. et al. (2017), 'Quantitative microbiome profiling links gut community variation to microbial load', *Nature* **551**(7681), 507–511.
- Wilson, S. (2022), 'Parbayesianoptimization: Parallel bayesian optimization of hyperparameters', <https://cran.r-project.org/web/packages/ParBayesianOptimization/index.html>.
- Wood, S. N. (2017), *Generalized additive models: an introduction with R*, Chapman and Hall/CRC.

# Supplement Materials of Scalable Bayesian Semiparametric Additive Regression Models For Microbiome Studies

Tinghua Chen

College of Information Science and Technology,  
Pennsylvania State University

and

Michelle Pistner Nixon

College of Information Science and Technology,  
Pennsylvania State University

and

Justin D. Silverman

College of Information Science and Technology,  
Department of Statistics,  
Department of Medicine,  
Pennsylvania State University

May 27, 2025

## 1 Review of the Collapsed-Uncollapsed (CU) Sampler

The definition of MLTPs is key to efficient inference. If a model  $p(\mathbf{Y}, \mathbf{H}, \Phi)$  has a closed-form marginal  $p(\mathbf{Y}, \mathbf{H})$  that is an LTP, then its closed form conditional  $p(\Phi | \mathbf{Y}, \mathbf{H})$  likely exists.

We call the marginal  $p(\mathbf{Y}, \mathbf{H})$  the *collapsed form* and  $p(\Phi | \mathbf{Y}, \mathbf{H})$  the *uncollapsed form*.

The posterior of an MLTP factors as

$$p(\mathbf{H}, \Phi | \mathbf{Y}) = p(\Phi | \mathbf{H}, \mathbf{Y})p(\mathbf{H} | \mathbf{Y})$$

with the uncollapsed form as the first term and the posterior of the collapsed form as the second. As the collapsed form is rarely conjugate, techniques such as MCMC can be used to obtain samples from its posterior. Then, conditioned on those samples, the uncollapsed form can be used to obtain samples from the joint posterior. Especially when  $\Phi$  is high-dimensional, this *Collapse-Uncollapse* sampler can be much more efficient than common alternatives (?). Still, the most substantial enhancements occur when approximations to the collapsed form are considered.

We have developed a Laplace approximation for the collapsed form of MLTPs:

$$p(\text{vec}(\mathbf{H}) \mid \mathbf{Y}) \approx \mathcal{N}(\text{vec}(\hat{\mathbf{H}}), \nabla^{-2}[\text{vec}(\hat{\mathbf{H}})])$$

where  $\hat{\mathbf{H}}$  denotes the *Maximum A Posteriori (MAP)* estimate of the collapsed form and  $\nabla^{-2}[\text{vec}(\hat{\mathbf{H}})]$  denotes the inverse Hessian of the collapsed form evaluated at the MAP estimate. The derived analytical results for the gradient and Hessian of the collapsed form is in Supplement section 3. Focusing on applications to MultiAddGPs, we proved error bounds on the Laplace approximation and provided simulation and real analyses showing that the approximation was extremely accurate in the context of microbiome data analysis. Beyond the accuracy of posterior calculations, we showed that this CU sampler with the Laplace approximation (simply referred to as the CU sampler in the following text) was often 4-5 orders of magnitude faster than MCMC and 1-2 orders of magnitude faster than black-box variational inference while also being more accurate than the later.

## 2 MultiAddGPs as Marginal Latent Matrix-t Process (MLTPs)

### 2.1 Derivation of Collapsed form

**Theorem 2.1.** *MultiAddGPs are MLTPs with parameters  $\Phi = \{\mathbf{F}, \mathbf{B}, \mathbf{f}^{(1)}, \dots, \mathbf{f}^{(K)}, \Sigma\}$ .*

*The collapsed form  $p(\mathbf{Y}, \mathbf{H})$  is an LTP:*

$$\mathbf{Y}_{\cdot n} \sim \text{Multinomial}(\mathbf{\Pi}_{\cdot n})$$

$$\mathbf{\Pi}_{\cdot n} = \phi^{-1}(\mathbf{H}_{\cdot n})$$

$$\mathbf{H} \sim TP(\nu, \mathbf{M}, \mathbf{V}, \mathbf{A})$$

where  $\phi$  is an invertible log-ratio transformation,  $\mathbf{M} = \Theta^{(0)}\mathbf{X} + \sum_{k=1}^K \Theta^{(k)}(\mathbf{Z}^{(k)})$ ,  $\mathbf{V} = \Xi$ , and  $\mathbf{A} = \mathbf{X}^T \Gamma^{(0)} \mathbf{X} + \sum_{k=1}^K \Gamma^{(k)}(\mathbf{Z}^{(k)}) + \mathbf{I}_N$ ,  $\nu = \zeta$

*Proof.* We prove this theorem by showing that the marginal of MultiAddGP models is an LTP. By definition 2 from (?), if  $p(\mathbf{H}, \mathbf{Y})$  is an LTP, then  $p(\mathbf{H}, \mathbf{Y}, \mathbf{F}, \mathbf{f}^{(1)}, \dots, \mathbf{f}^{(K)}, \Sigma)$  is a MLTP model. To begin with, we note that Equation (4) in the main text (along with its priors) can alternatively be written as:

$$\mathbf{H} = \mathbf{F} + \mathbf{E}^{\mathbf{H}} \quad \mathbf{E}^{\mathbf{H}} \sim N(0, \Sigma, \mathbf{I}_N) \quad (1)$$

$$\mathbf{F} = \mathbf{B}\mathbf{X} + \sum_{k=1}^K \mathbf{f}^{(k)}(\mathbf{Z}^{(k)}) \quad (2)$$

$$\mathbf{B} = \Theta^{(0)} + \mathbf{E}^{\mathbf{B}} \quad \mathbf{E}^{\mathbf{B}} \sim N(0, \Sigma, \Gamma^{(0)}) \quad (3)$$

$$\mathbf{f}^{(k)} = \Theta^{(k)} + \mathbf{E}^{\mathbf{f}^{(k)}} \quad \mathbf{E}^{\mathbf{f}^{(k)}} \sim N(0, \Sigma, \Gamma^{(k)}) \quad (4)$$

$$\Sigma \sim IW(\Xi, \zeta) \quad (5)$$

Using this form in combination with the affine transformation property of the matrix normal distribution, it is straightforward to marginalize over  $\mathbf{B}$  and  $\mathbf{f}^{(k)}$  producing the following

form:

$$\mathbf{F} = \Theta^{(0)}\mathbf{X} + \sum_{k=1}^K \Theta^{(k)}(\mathbf{Z}^{(k)}) + \mathbf{E}^{\mathbf{B}} + \mathbf{E}^{\mathbf{f}^{(k)}} \quad \mathbf{E}^{\mathbf{B}} \sim N(0, \Sigma, \Gamma^{(0)}) \quad \mathbf{E}^{\mathbf{f}^{(k)}} \sim N(0, \Sigma, \Gamma^{(k)}) \quad (6)$$

$$\mathbf{F} = \Theta^{(0)}\mathbf{X} + \sum_{k=1}^K \Theta^{(k)}(\mathbf{Z}^{(k)}) + \mathbf{E}^{\mathbf{F}} \quad \mathbf{E}^{\mathbf{F}} \sim N(0, \Sigma, \mathbf{X}^T \Gamma^{(0)} \mathbf{X} + \sum_{k=1}^K \Gamma^{(k)}(\mathbf{Z}^{(k)})) \quad (7)$$

Thus we may rewrite Equations (1) - (5) as

$$\mathbf{H} = \mathbf{F} + \mathbf{E}^{\mathbf{H}} \quad \mathbf{E}^{\mathbf{H}} \sim N(0, \Sigma, \mathbf{I}_N) \quad (8)$$

$$\mathbf{F} = \Theta^{(0)}\mathbf{X} + \sum_{k=1}^K \Theta^{(k)}(\mathbf{Z}^{(k)}) + \mathbf{E}^{\mathbf{F}} \quad \mathbf{E}^{\mathbf{F}} \sim N(0, \Sigma, \mathbf{X}^T \Gamma^{(0)} \mathbf{X} + \sum_{k=1}^K \Gamma^{(k)}(\mathbf{Z}^{(k)})) \quad (9)$$

$$\Sigma \sim IW(\Xi, \zeta) \quad (10)$$

Following the result from ?, we can marginalize over  $\mathbf{F}$  and  $\Sigma$  in Equations (9) and (10) to get

$$\mathbf{H} \sim TP(\zeta, \Theta^{(0)}\mathbf{X} + \sum_{k=1}^K \Theta^{(k)}(\mathbf{Z}^{(k)}), \Xi, \mathbf{X}^T \Gamma^{(0)} \mathbf{X} + \sum_{k=1}^K \Gamma^{(k)}(\mathbf{Z}^{(k)}) + \mathbf{I}_N)$$

Finally, incorporating Equations (2) and (3) allows us to write the marginalized form of the MultiAddGP model as an LTP

$$\mathbf{Y} \sim g(\mathbf{\Pi}, \lambda)$$

$$\mathbf{\Pi} = \phi^{-1}(\mathbf{H})$$

$$\mathbf{H} \sim TP(\nu, \mathbf{M}, \mathbf{V}, \mathbf{A}).$$

where  $g$  is product multinomial,  $\phi$  is an invertible log-ratio transformation,  $\mathbf{M} = \Theta^{(0)}\mathbf{X} + \sum_{k=1}^K \Theta^{(k)}(\mathbf{Z}^{(k)})$ ,  $\mathbf{V} = \Xi$ , and  $\mathbf{A} = \mathbf{X}^T \Gamma^{(0)} \mathbf{X} + \sum_{k=1}^K \Gamma^{(k)}(\mathbf{Z}^{(k)}) + \mathbf{I}_N$ ,  $\nu = \zeta$   $\square$

## 2.2 Derivation of Uncollapsed form - Sample from $p(\mathbf{F}, \Sigma | \mathbf{H}, \mathbf{Y})$

Here, we demonstrate how to efficiently compute and sample from the conditional posterior  $p(\mathbf{F}, \Sigma | \mathbf{H}, \mathbf{Y}, \mathbf{X}, \mathbf{Z})$ . Since  $\mathbf{F}$  and  $\Sigma$  are conditionally independent of  $\mathbf{Y}$  given  $\mathbf{H}$ , by applying

the chain rule, we can rewrite the equation as:

$$p(\mathbf{F}, \Sigma | \mathbf{H}, \mathbf{Y}, \mathbf{X}, \mathbf{Z}) = p(\mathbf{F} | \Sigma, \mathbf{H}, \mathbf{X}, \mathbf{Z}) p(\Sigma | \mathbf{H}, \mathbf{X}, \mathbf{Z})$$

To proceed, we clarify the notation used to distinguish between *smoothing* and *prediction*.

Smoothing refers to inferring latent quantities over observed covariates  $(\mathbf{X}^o, \mathbf{Z}^o)$ , while

prediction refers to inferring latent quantities over unobserved covariates  $(\mathbf{X}^u, \mathbf{Z}^u)$ . We thus

define the expanded notation:

$$\begin{aligned} \mathbf{X} &= \begin{bmatrix} \mathbf{X}^o & \mathbf{X}^u \end{bmatrix}, & \mathbf{Z} &= \begin{bmatrix} \mathbf{Z}^o & \mathbf{Z}^u \end{bmatrix}, \\ \Sigma &= \begin{bmatrix} \Sigma^{oo} & (\Sigma^{uo})^T \\ \Sigma^{uo} & \Sigma^{uu} \end{bmatrix}, & \mathbf{F} &= \begin{bmatrix} \mathbf{F}^o & \mathbf{F}^u \end{bmatrix}, \\ \Theta &= \begin{bmatrix} \Theta^o & \Theta^u \end{bmatrix}, & \Gamma &= \begin{bmatrix} \Gamma^{oo} & (\Gamma^{uo})^T \\ \Gamma^{uo} & \Gamma^{uu} \end{bmatrix}. \end{aligned}$$

where

$$\begin{aligned} \Theta^o &= \Theta^{(0)} \mathbf{X}^o - \sum_{k=1}^K \Theta^{(k)}(\mathbf{Z}^{(k),o}), \\ \Theta^u &= \Theta^{(0)} \mathbf{X}^u - \sum_{k=1}^K \Theta^{(k)}(\mathbf{Z}^{(k),u}), \\ \Gamma^{oo} &= \mathbf{X}^{T,o} \Gamma^{(0)} \mathbf{X}^o + \sum_{k=1}^K \Gamma^{(k)}(\mathbf{Z}^{(k),o}), \\ \Gamma^{uu} &= \mathbf{X}^{T,u} \Gamma^{(0)} \mathbf{X}^u + \sum_{k=1}^K \Gamma^{(k)}(\mathbf{Z}^{(k),u}), \\ \Gamma^{uo} &= \mathbf{X}^T \Gamma^{(0)} \mathbf{X} + \sum_{k=1}^K \Gamma^{(k)}(\mathbf{Z}^{(k),o}, \mathbf{Z}^{(k),u}). \end{aligned}$$

Let  $D = D_o + D_u$  and  $N = N_o + N_u$  denote the total dimensionality of  $\Sigma$  and  $\Gamma$ . To

sample from  $p(\mathbf{F} | \Sigma, \mathbf{H}, \mathbf{X}, \mathbf{Z})$  and  $p(\Sigma | \mathbf{H}, \mathbf{X}, \mathbf{Z})$ , we define:  $\Sigma^{ou/oo} = (\Sigma^{oo})^{-1} (\Sigma^{uo})^T$  and

$\Sigma^{uu \cdot oo} = \Sigma^{uu} - \Sigma^{uo} \Sigma^{ou/oo}$ . and using the conditional properties of the inverse-Wishart

distribution ?, we sample  $\Sigma$  and  $\mathbf{F}$  from following:

$$\begin{aligned}\Sigma^{uu \cdot oo} &\sim \mathcal{IW}(\Xi^{uu \cdot oo}, \zeta + D), \\ \Sigma^{ou/oo} \mid \Sigma^{uu \cdot oo} &\sim \mathcal{N}(\Xi^{ou/oo}, (\Xi^{oo})^{-1}, \Sigma^{uu \cdot oo}), \\ \Sigma &= \begin{bmatrix} (\Sigma^{oo})^{-1} + \Sigma^{ou/oo}(\Sigma^{uu \cdot oo})^{-1}(\Sigma^{ou/oo})^T & -\Sigma^{ou/oo}(\Sigma^{uu \cdot oo})^{-1} \\ -(\Sigma^{uu \cdot oo})^{-1}(\Sigma^{ou/oo})^T & (\Sigma^{uu \cdot oo})^{-1} \end{bmatrix}, \\ \mathbf{F}^u \mid \mathbf{F}^o, \Sigma &\sim \mathcal{N}(\Theta^u + (\mathbf{F}^o - \Theta^o)\Gamma^{ou/oo}, \Sigma, \Gamma^{uu} - \Gamma^{uo}(\Gamma^{oo})^{-1}\Gamma^{ou}).\end{aligned}$$

### 3 Laplace Approximation in the Collapsed Step

The Laplace approximation for the collapsed step involves three main steps: (1) obtaining the MAP estimate  $\hat{\mathbf{H}}$  via optimization, (2) computing the Hessian matrix  $\nabla^{-2}\text{vec}(\hat{\mathbf{H}})$  at the MAP estimate, and (3) sampling from the approximating Gaussian distribution  $\mathcal{N}(\text{vec}(\hat{\mathbf{H}}), \nabla^{-2}(\text{vec}\hat{\mathbf{H}}))$ . The MAP estimate of  $\mathbf{H}$  is obtained by solving the following optimization problem:

$$\begin{aligned}\hat{\mathbf{H}} &= \arg \min_{\mathbf{H}} \{\log p(\mathbf{H} \mid \mathbf{Y})\} \\ &\propto \arg \min_{\mathbf{H}} \{-\log g(\mathbf{Y} \mid \phi^{-1}(\mathbf{H})) - \log p(\mathbf{H})\}.\end{aligned}$$

We use the L-BFGS optimizer to solve this problem, which requires computing the gradient of the negative log-posterior:

$$-\frac{d \log p(\mathbf{H} \mid \mathbf{Y})}{d\text{vec}(\mathbf{H})} = -\frac{d \log g(\mathbf{Y} \mid \phi^{-1}(\mathbf{H}))}{d\text{vec}(\mathbf{H})} - \frac{d \log p(\mathbf{H})}{d\text{vec}(\mathbf{H})}.$$

The two gradient components are computed as follows:

$$-\frac{d \log g(\mathbf{Y} \mid \phi^{-1}(\mathbf{H}))}{d\text{vec}(\mathbf{H})} = \left( \text{vec}(\mathbf{Y}) - \text{vec}(I_D I_D^T \mathbf{Y}) \odot \mathbf{J} \right)^T, \quad (11)$$

$$-\frac{d \log p(\mathbf{H})}{d\text{vec}(\mathbf{H})} = \text{vec} \left( (\mathbf{R} + \mathbf{R}^T) \mathbf{C}^T \right)^T, \quad (12)$$

where:

$$\begin{aligned}
J &= \text{vec}(\exp(\mathbf{H})) \oslash \text{vec}\left(I_{D-1}(I + \exp(\mathbf{H})^T I_{D-1})^T\right), \\
\mathbf{R} &= \left(I_P + \mathbf{V}^{-1}(\mathbf{H} - \mathbf{M})\mathbf{A}^{-1}(\mathbf{H} - \mathbf{M})^T\right)^{-1} \mathbf{V}^{-1}, \\
\mathbf{C} &= \mathbf{A}^{-1}(\mathbf{H}^T - \mathbf{M}^T).
\end{aligned}$$

Once the MAP estimate  $\hat{\mathbf{H}}$  has been obtained, we compute the Hessian at that point:

$$\nabla^{-2}[\hat{\mathbf{H}}] = \nabla^{-2} \log g(\mathbf{Y} \mid \phi^{-1}(\hat{\mathbf{H}})) + \nabla^{-2} \log p(\hat{\mathbf{H}}).$$

Using equations (11) and (12), the Hessians of the likelihood and prior terms are given by:

$$\begin{aligned}
\nabla^{-2} \log g(\mathbf{Y} \mid \phi^{-1}(\mathbf{H})) &= \text{diag}(W^{(1)}, \dots, W^{(N)}), \\
\nabla^{-2} \log p(\mathbf{H}) &= \left(A^{-1} \otimes (R + R^T)\right) - (L + L^T) \\
&\quad - T_{N,D-1} \left[ (RC^T \otimes CR^T) + (R^T C^T \otimes CR) \right],
\end{aligned}$$

where:

$$\begin{aligned}
W^{(j)} &= I_D^T Y \left( J_{(j)} J_{(j)}^T - \text{diag}(J_{(j)}) \right), \\
L &= \mathbf{C} \mathbf{R} \mathbf{C}^T \otimes \mathbf{R}^T,
\end{aligned}$$

and  $T_{N,D-1}$  is an  $N(D-1) \times N(D-1)$  permutation matrix. Finally, we draw samples from the approximating Gaussian distribution. The Laplace approximation to the posterior  $p(\mathbf{H} \mid \mathbf{Y})$  is given by:

$$q(\mathbf{H} \mid \mathbf{Y}) = \mathcal{N}(\text{vec}(\hat{\mathbf{H}}), \nabla^{-2}(\text{vec} \hat{\mathbf{H}})).$$

In practice, to avoid explicit matrix inversion when sampling, we apply the Cholesky decomposition of the Hessian.

## 4 Derivation of the posterior distribution of Matrix Normal

**Theorem 4.1.** *If*

$$\mathbf{Y} \mid \mathbf{\Lambda} \sim \mathcal{MN}(\mathbf{\Lambda}\mathbf{X}, \mathbf{\Sigma}, \mathbf{\Gamma})$$

$$\mathbf{\Lambda} \sim \mathcal{MN}(\mathbf{\Theta}, \mathbf{\Sigma}, \mathbf{Z})$$

and  $\mathbf{\Sigma}$  is known, then the posterior of  $\mathbf{\Lambda}$  is given by:

$$\mathbf{\Lambda} \mid \mathbf{\Sigma}, \mathbf{Y} \sim \mathcal{MN}\left((\mathbf{Y}\mathbf{\Gamma}^{-1}\mathbf{X}^T + \mathbf{\Theta}\mathbf{Z}^{-1})(\mathbf{X}\mathbf{\Gamma}^{-1}\mathbf{X}^T + \mathbf{Z}^{-1})^{-1}, \mathbf{\Sigma}, (\mathbf{X}\mathbf{\Gamma}^{-1}\mathbf{X}^T + \mathbf{Z}^{-1})^{-1}\right)$$

*Proof.* Using the density function of the matrix normal distribution, we can write:

$$\mathbf{\Lambda} \mid \mathbf{Y} \propto \exp\left[-\frac{1}{2}\text{tr}\left(\mathbf{\Sigma}^{-1}(\mathbf{Y} - \mathbf{\Lambda}\mathbf{X})\mathbf{\Gamma}^{-1}(\mathbf{Y} - \mathbf{\Lambda}\mathbf{X})^T\right)\right] \times \exp\left[-\frac{1}{2}\text{tr}\left(\mathbf{\Sigma}^{-1}(\mathbf{\Lambda} - \mathbf{\Theta})\mathbf{Z}^{-1}(\mathbf{\Lambda} - \mathbf{\Theta})^T\right)\right]$$

Combining the exponents and expanding the term:

$$\begin{aligned} \propto \exp\left[-\frac{1}{2}\text{tr}\left(\mathbf{\Sigma}^{-1}\left(\mathbf{Y}\mathbf{\Gamma}^{-1}\mathbf{Y}^T - \mathbf{\Lambda}\mathbf{X}\mathbf{\Gamma}^{-1}\mathbf{Y}^T - \mathbf{Y}\mathbf{\Gamma}^{-1}\mathbf{X}^T\mathbf{\Lambda}^T + \mathbf{\Lambda}\mathbf{X}\mathbf{\Gamma}^{-1}\mathbf{X}^T\mathbf{\Lambda}^T \right. \right. \\ \left. \left. + \mathbf{\Lambda}\mathbf{Z}^{-1}\mathbf{\Lambda}^T - \mathbf{\Theta}\mathbf{Z}^{-1}\mathbf{\Lambda}^T - \mathbf{\Lambda}\mathbf{Z}^{-1}\mathbf{\Theta}^T + \mathbf{\Theta}\mathbf{Z}^{-1}\mathbf{\Theta}^T\right)\right]. \end{aligned}$$

$$\begin{aligned} \propto \exp\left[-\frac{1}{2}\text{tr}\left(\mathbf{\Sigma}^{-1}\left(-\mathbf{\Lambda}\mathbf{X}\mathbf{\Gamma}^{-1}\mathbf{Y}^T - \mathbf{Y}\mathbf{\Gamma}^{-1}\mathbf{X}^T\mathbf{\Lambda}^T + \mathbf{\Lambda}\mathbf{X}\mathbf{\Gamma}^{-1}\mathbf{X}^T\mathbf{\Lambda}^T + \mathbf{\Lambda}\mathbf{Z}^{-1}\mathbf{\Lambda}^T \right. \right. \\ \left. \left. - \mathbf{\Theta}\mathbf{Z}^{-1}\mathbf{\Lambda}^T - \mathbf{\Lambda}\mathbf{Z}^{-1}\mathbf{\Theta}^T\right)\right] \end{aligned}$$

Grouping like terms:

$$\begin{aligned} \mathbf{\Lambda} \mid \mathbf{Y} \propto \exp\left[-\frac{1}{2}\text{tr}\left(\mathbf{\Sigma}^{-1}\left(\mathbf{\Lambda}(\mathbf{X}\mathbf{\Gamma}^{-1}\mathbf{X}^T + \mathbf{Z}^{-1})\mathbf{\Lambda}^T - \mathbf{\Lambda}(\mathbf{X}\mathbf{\Gamma}^{-1}\mathbf{Y}^T + \mathbf{Z}^{-1}\mathbf{\Theta}^T) - (\mathbf{Y}\mathbf{\Gamma}^{-1}\mathbf{X}^T + \mathbf{\Theta}\mathbf{Z}^{-1})\mathbf{\Lambda}^T\right)\right)\right] \\ \propto \exp\left(-\frac{1}{2}\text{tr}\left\{\mathbf{\Sigma}^{-1}\left((\mathbf{\Lambda} - (\mathbf{Y}\mathbf{\Gamma}^{-1}\mathbf{X}^T - \mathbf{\Theta}\mathbf{Z}^{-1})(\mathbf{X}\mathbf{\Gamma}^{-1}\mathbf{X}^T + \mathbf{Z}^{-1})^{-1}) \right. \right. \right. \\ \left. \left. \times (\mathbf{X}\mathbf{\Gamma}^{-1}\mathbf{X}^T + \mathbf{Z}^{-1})\left(\mathbf{\Lambda} - (\mathbf{Y}\mathbf{\Gamma}^{-1}\mathbf{X}^T - \mathbf{\Theta}\mathbf{Z}^{-1})(\mathbf{X}\mathbf{\Gamma}^{-1}\mathbf{X}^T + \mathbf{Z}^{-1})^{-1}\right)^T\right)\right\}\right). \end{aligned}$$

which implies that

$$\Lambda \mid \Gamma, \mathbf{Y} \sim \mathcal{MN}\left((\mathbf{Y}\Gamma^{-1}\mathbf{X}^T - \Theta\mathbf{Z}^{-1})(\mathbf{X}\Gamma^{-1}\mathbf{X}^T + \mathbf{Z}^{-1})^{-1}, \Sigma, (\mathbf{X}\Gamma^{-1}\mathbf{X}^T + \mathbf{Z}^{-1})^{-1}\right)$$

□

Note that in the special case where  $\mathbf{X} = \mathbf{I}$ , i.e., a model of the form:

$$\mathbf{Y} \mid \Lambda \sim \mathcal{MN}(\Lambda, \Sigma, \Gamma)$$

$$\Lambda \sim \mathcal{MN}(\Theta, \Sigma, \mathbf{Z})$$

then the above result simplifies to

$$\Lambda \mid \Sigma, \mathbf{Y} \sim \mathcal{MN}\left((\mathbf{Y}\Gamma^{-1} + \Theta\mathbf{Z}^{-1})(\Gamma^{-1} + \mathbf{Z}^{-1})^{-1}, \Sigma, (\Gamma^{-1} + \mathbf{Z}^{-1})^{-1}\right).$$

## 5 Simulation study

### 5.1 Simulation 1

To evaluate the implementation and investigate the behavior of the MultiAddGPs model, we simulated a synthetic microbial community time-series comprising four bacterial taxa across 600 time points, based on the following model:

$$\mathbf{f}^{(\text{periodic})}(t_n) \sim \mathcal{MN}(0, \Sigma, \Gamma^{(\text{periodic})})$$

$$\mathbf{f}^{(\text{trend})}(t_n) \sim \mathcal{MN}(0, \Sigma, \Gamma^{(\text{trend})})$$

$$\mathbf{F}_{.n} = 2.7 + 3x_n^{(\text{batch})} + \mathbf{f}^{(\text{periodic})}(t_n) + \mathbf{f}^{(\text{trend})}(t_n)$$

$$\mathbf{\Pi}_{.n} = ALR^{-1}(\mathbf{H})$$

$$\mathbf{Y}_{.n} \sim \text{Multinomial}(\mathbf{\Pi}_{.n})$$

Here, we set  $\Sigma$  as a covariance matrix with off-diagonal elements of 0.9 and diagonal elements of 1.5. The periodic kernel is defined as  $\Gamma^{(\text{periodic})} = 4 \exp\left(-\frac{2 \sin^2\left(\frac{\pi|t-t'|}{25}\right)}{30^2}\right)$ , while the trend kernel is modeled as  $\Gamma^{(\text{trend})} = \exp\left(-\frac{(t-t')^2}{2 \times 30^2}\right)$ . After obtaining the posterior samples from the MultiAddGPs model, we apply a sum-to-zero constraint to facilitate model identification.

In Figure 1 of the main text, we illustrate the model’s ability to successfully decompose the simulated microbiome time-series for a single taxon. In Figures 1 and 2 in the supplementary section, we further demonstrate this decomposition for two additional taxa.

Next, we assessed the scalability of the model. However, as the dimensions ( $D$ ) and number of time points ( $N$ ) increased, it became increasingly challenging to simulate data with a distinct non-linear trend suitable for additive modeling. To address this, we replaced the non-linear trend kernel  $\Gamma^{(\text{trend})}$  with a linear kernel:  $\Gamma^{(\text{trend})} = 20^2 + (t - c)(t' - c)$ , while keeping the rest of the model unchanged. We then simulated this modified model across various combinations of  $D$  and  $N$ , where  $D \in 3, \dots, 100$  and  $N \in 50, \dots, 1000$ . For each combination of  $(D, N)$ , we generated three simulated datasets. The coverage ratio, presented in Figure 2 of the main text, represents the average across these three simulations.

Analysis of the simulated dataset revealed that the estimates for the unobserved compositions,  $\mathbf{H}$ , and latent factors,  $\mathbf{F}$ , obtained from the MultiAddGPs model were more accurate compared to those derived from the standard approach of normalizing read counts to proportions (NAddGPs). Furthermore, our model successfully disentangled distinct effects arising from multiple linear and non-linear factors. These results suggest that our model is capable of effectively decomposing longitudinal microbiota data into a mixture of linear and non-linear additive components.

All implements were compiled and run using gcc version 9.1.0 and R version 4.3.2. All replicates of the simulated count data were supplied to the various implementations independently and the models were fit on identical hardware, allotted 64GB RAM, 4 cores, and restricted

to a 48-hour upper limit on run-time.

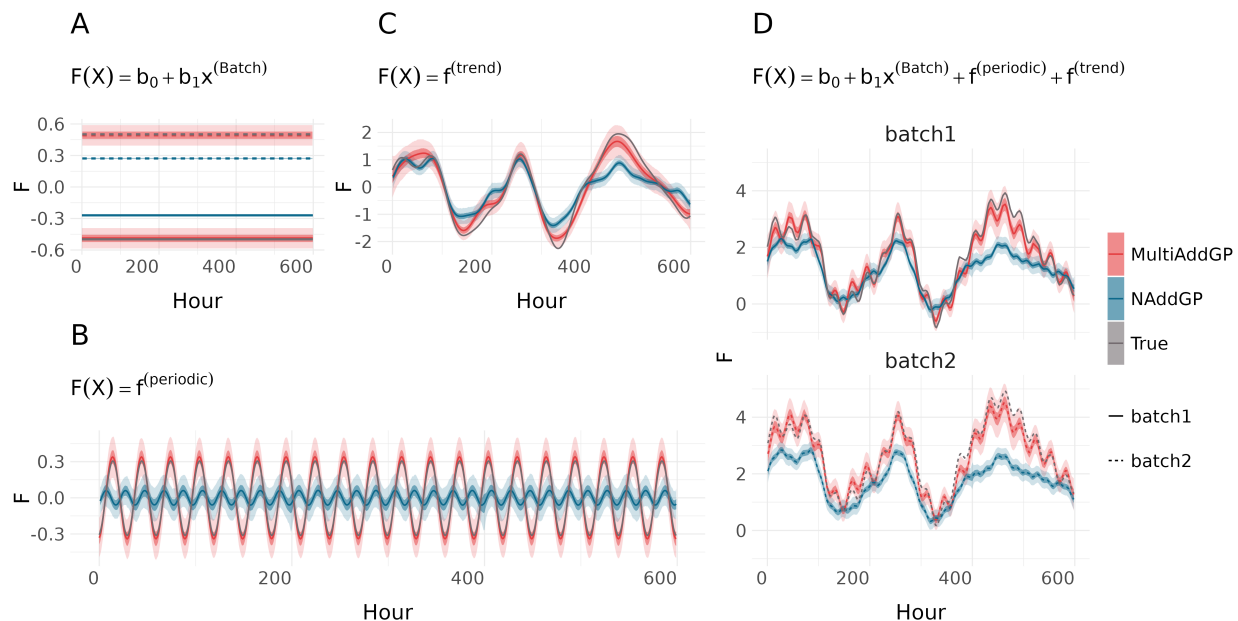


Figure 1: MultiAddGPs successfully decompose simulated microbiome time-series on Taxa

2.

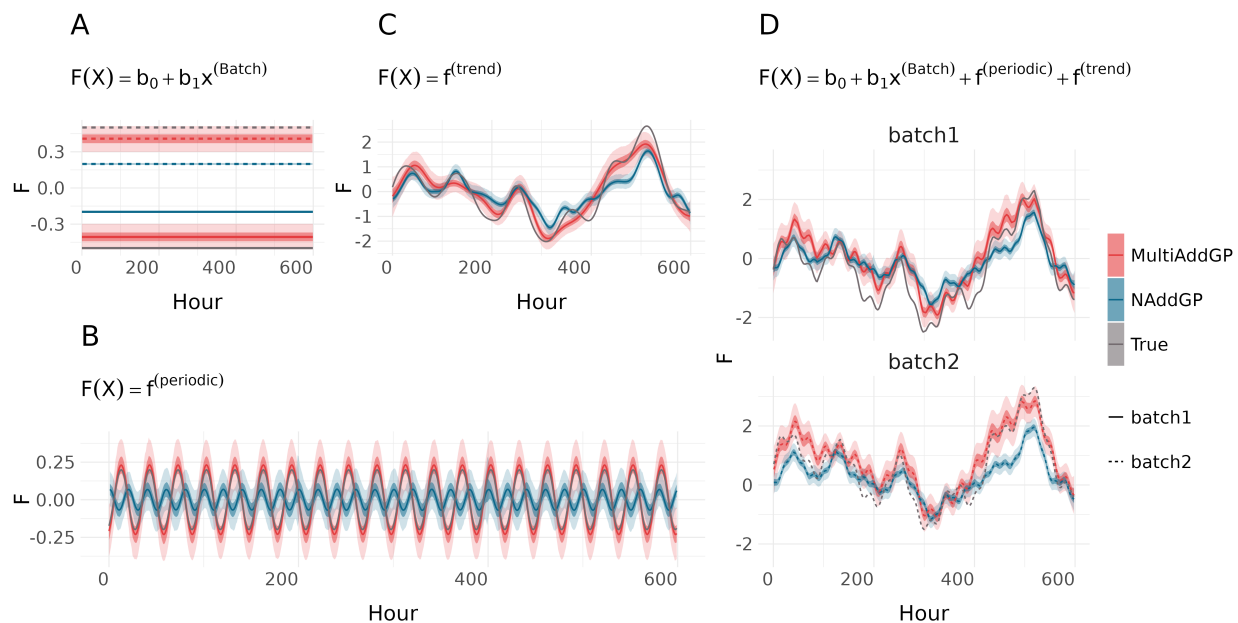


Figure 2: MultiAddGPs successfully decompose simulated microbiome time-series on Taxa

3.

## 5.2 Simulation 2

To evaluate the performance of our model relative to the existing method *Lgpr* (?), we conducted a simulation study. Since *Lgpr* does not scale to larger datasets, we generated a small dataset with  $D = 3$  and  $N = 50$  for inference comparison. The simulation follows the model:

$$\begin{aligned} \mathbf{f}^{(\text{non-stationary})}(w_n) &\sim \mathcal{MN}(0, \Sigma, \mathbf{\Gamma}^{(\text{non-stationary})}) \\ \mathbf{f}^{(\text{trend})}(t_n) &\sim \mathcal{MN}(0, \Sigma, \mathbf{\Gamma}^{(\text{trend})}) \\ \mathbf{F}.n &= 0.4 + x_n^{(\text{batch})} + \mathbf{f}^{(\text{non-stationary})}(w_n) + \mathbf{f}^{(\text{trend})}(t_n) \\ \mathbf{\Pi}.n &= ALR^{-1}(\mathbf{H}) \\ \mathbf{Y}.n &\sim \text{Multinomial}(\mathbf{\Pi}.n) \end{aligned}$$

Here,  $w_n$  is a transformed skewed Gaussian of input  $t_n$ , used in the non-stationary kernel model:

$$\begin{aligned} z_n &= \frac{t_n - m}{s} \\ w_n &= \exp\left(\frac{1}{2}z_n^2\right) \times \frac{1}{1 + \exp(-\alpha z_n)} \end{aligned}$$

where  $m$  determines the peak location of the distribution,  $s$  controls its width, and  $\alpha$  is the skew parameter. When  $\alpha = 0$ , the function reduces to a standard Gaussian; positive  $\alpha$  induces a heavier right tail, while negative  $\alpha$  results in a heavier left tail. In this simulation, the covariance matrix  $\Sigma$  is set with off-diagonal elements of 0.5 and diagonal elements of 1. The non-stationary kernel is defined as  $\mathbf{\Gamma}^{(\text{non-stationary})} = 2 \times \exp\left(-\frac{(t-t')^2}{2 \times 3^2}\right)$ , while the general kernel is modeled as  $\mathbf{\Gamma}^{(\text{trend})} = \exp\left(-\frac{(t-t')^2}{2 \times 0.5^2}\right)$ . As in Simulation 1, we apply a sum-to-zero constraint to facilitate model identification after obtaining posterior samples from both models.

Since *Lgpr* utilizes predefined kernels, we aimed to select the most appropriate kernel configurations to closely align with their model structure. The *Lgpr* model was fitted

using the `lgp` function with a structured formula. Specifically, the response variable  $Y$  was modeled as a function of an interaction term between zero-sum kernel:  $zs(\text{ID})$  and a Gaussian process over time:  $gp(t_n)$ , designed to capture long-term temporal trends. To model batch effects, we employed their sum-zero kernel for categorical variables,  $zs(x_n^{\text{batch}})$ .  $gp\_ns(t_n)$  was used for modeling the non-stationary effect. A negative binomial ("nb") likelihood was specified, and the prior distribution were set as follows: a normal prior  $\mathcal{N}(2, 1)$  for the  $\alpha$  parameter, a normal prior  $\mathcal{N}(0.8, 1)$  for the length scale  $\ell$ , and a log-normal prior  $\log\mathcal{N}(1, 1)$  for the warping parameter. The model was trained using 5000 iterations across 4 MCMC chains, with a refresh interval of 2000. To improve sampling efficiency, the control settings included an adaptation delta of 0.999 and a maximum tree depth of 11.

Figure 3 presents the inference performance of the two models in Simulation 2. While the uncertainty estimates of the Lgpr model includes the true values, the associated uncertainty is excessively wide, which makes it ineffective in capturing the underlying pattern and providing meaningful insights. In contrast, MultiAddGPs accurately capture the true pattern with significantly lower uncertainty. Notably, the Lgpr model required approximately 7 hours to complete the analysis for a single taxon, whereas MultiAddGPs performed the same analysis for all taxa in under one minute.

## 6 Details on Artificial gut data application

We describe the specific MultiAddGPs model applied to the artificial gut dataset as a particular instance of the broader MultiAddGPs framework. Simplifications were introduced in three key areas: model structure, kernel selection, and prior specification.

First, regarding model structure, we analyzed four concurrent time-series from four artificial gut vessels. Given that the primary goal of our modeling was to isolate the effect of feed disruption, we represented the data as comprising two overlapping temporal processes: a

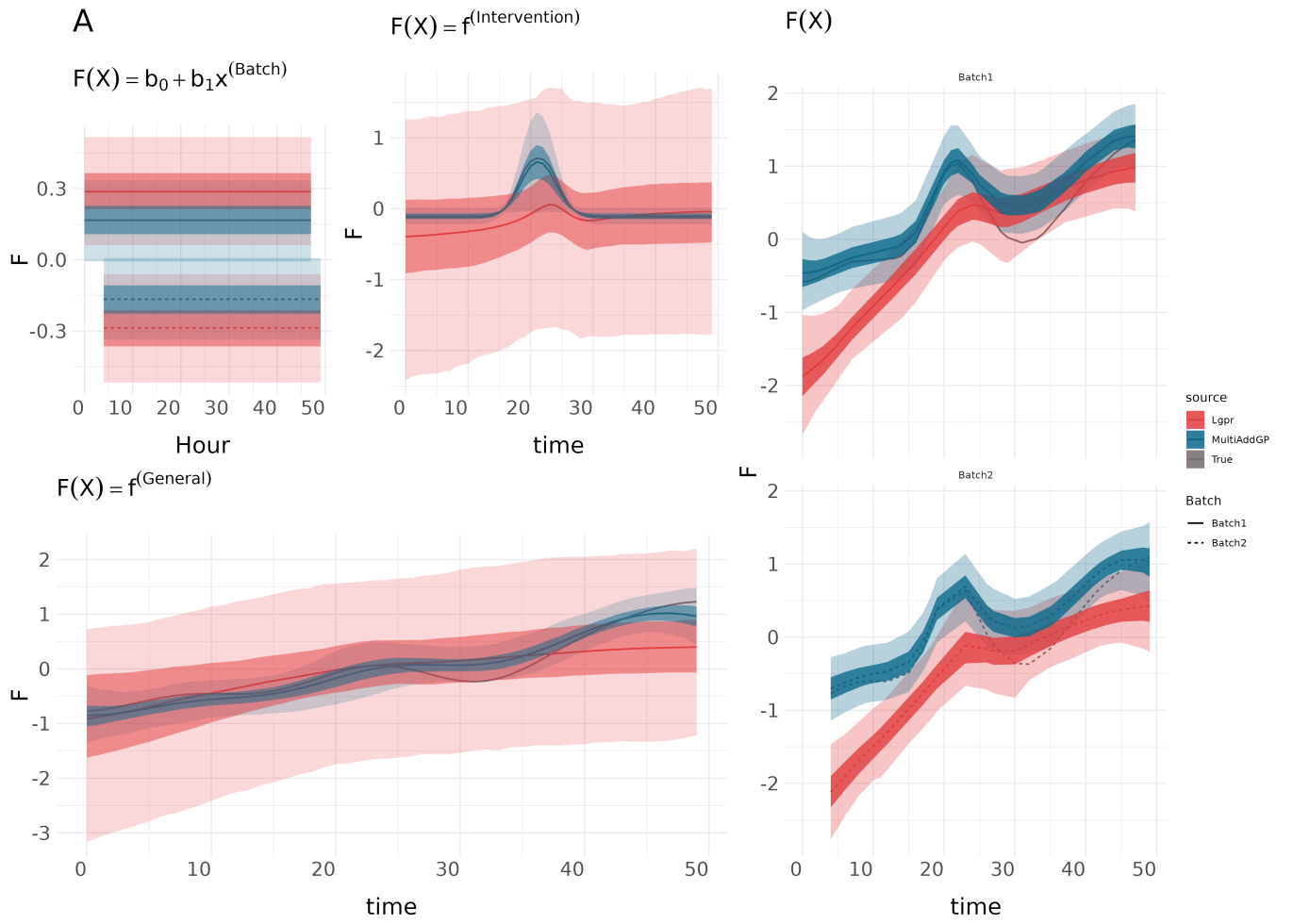


Figure 3: Inference comparison between MultiAddGPs and Lgpr

vessel-specific long-term trend,  $\mathbf{f}^{(\text{base},v)}$ , and a vessel-specific function capturing the effect of starvation,  $\mathbf{f}^{(\text{disrupt},v)}$ . Moreover, as the vessels were physically isolated from each other, we modeled them as independent processes by using block identity matrices  $\mathbf{\Gamma}^{(v)}$  such as:

$$\mathbf{\Gamma}^{(v)} \odot \mathbf{\Gamma}^{(\text{base})} = \begin{bmatrix} \mathbf{\Gamma}^{(v=1,\text{base})} & 0 & 0 & 0 \\ 0 & \mathbf{\Gamma}^{(v=2,\text{base})} & 0 & 0 \\ 0 & 0 & \mathbf{\Gamma}^{(v=3,\text{base})} & 0 \\ 0 & 0 & 0 & \mathbf{\Gamma}^{(v=4,\text{base})} \end{bmatrix}$$

$$\mathbf{\Gamma}^{(v)} \odot \mathbf{\Gamma}^{(\text{disrupt})} = \begin{bmatrix} \mathbf{\Gamma}^{(v=1,\text{disrupt})} & 0 \\ 0 & \mathbf{\Gamma}^{(v=2,\text{disrupt})} \end{bmatrix}$$

as the covariance structure of  $\mathbf{f}^{(\text{base},v)}$  and  $\mathbf{f}^{(\text{disrupt},v)}$ , where  $\odot$  represents the Kronecker product. To simplify prior specification, we standardized all continuous covariates (before fitting to the model) so that their means were zero and their standard deviations were one. All prior mean functions were set to the zero function. We use a squared exponential kernel to model long-term non-linear trends in  $\mathbf{\Gamma}^{(\text{base})}$ :

$$\mathbf{\Gamma}^{(\text{base})} = \sigma_{\text{base}}^2 \exp\left(-\frac{(t_n - t'_n)^2}{2\rho_{\text{base}}^2}\right)$$

For the disruption effects, we employ a rational quadratic kernel set to zero prior to day 11. This reflect the assumption that the target variable exhibits varying degrees of smoothness and irregularities near or after the starvation period:

$$\mathbf{\Gamma}^{(\text{disrupt})} = \sigma_{\text{disrupt}}^2 \left(1 + \frac{(t_n - t'_n)^2}{2a\rho_{\text{disrupt}}^2}\right)^{-a} \mathbf{I}(t_n \geq 11 \ \& \ t'_n \geq 11).$$

Regarding the prior settings for the hyperparameters, we specified two types of prior distributions for the parameters in the kernel functions: the prior over the length scale parameters  $(\rho_{\text{base}}, \rho_{\text{disrupt}})$  and the magnitude parameters  $(\sigma_{\text{base}}, \sigma_{\text{disrupt}})$  of the kernel. For both sets of parameters in each kernel, we adopted an InverseGamma distribution as follows:

$$\rho_{\text{base}}, \rho_{\text{disrupt}} \sim \text{InverseGamma}(\alpha_1, \beta_1)$$

$$\sigma_{\text{base}}, \sigma_{\text{disrupt}} \sim \text{InverseGamma}(\alpha_2, \beta_2)$$

with  $\alpha_1 = 10$ ,  $\beta_1 = 20$ ,  $\alpha_2 = 10$ ,  $\beta_2 = 10$  for  $\mathbf{\Gamma}^{(\text{base})}$ , and  $\alpha_1 = 10$ ,  $\beta_1 = 10$ ,  $\alpha_2 = 10$ ,  $\beta_2 = 20$  for  $\mathbf{\Gamma}^{(\text{disrupt})}$  (see Figure 4 for density plot). Note that we fixed the  $a$  parameter in the rational quadratic kernel, which determines the relative weighting of large-scale and small-scale variations, at a value of 2. These specification reflects our assumption that the model is constrained from learning distances that are significantly smaller or larger than the temporal distances among  $t$ . In other words, the prior penalizes extremely small or large

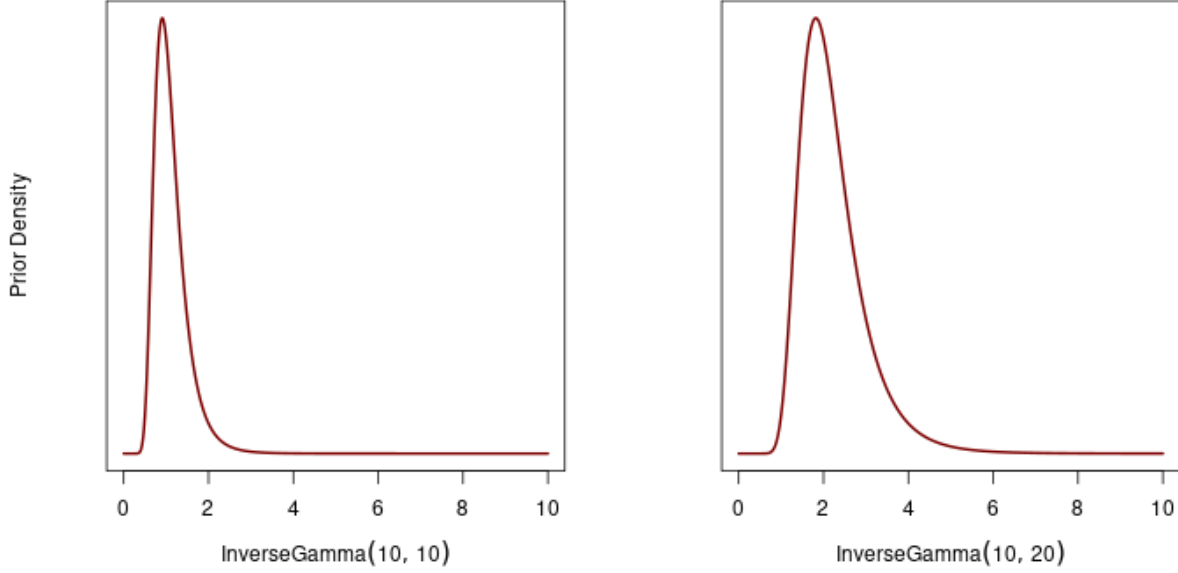


Figure 4: Prior density plots for the InverseGamma distributions used for the hyperparameters in the kernel functions (Artificial gut data)

length scales. The penalized marginal likelihood is given by

$$\begin{aligned} \log \int p(\mathbf{H}, \mathbf{Y} \mid \Omega) d\mathbf{H} &\approx \frac{(D-1)N}{2} \log(2\pi) + \log p(\hat{\mathbf{H}}_{\Omega}, \mathbf{Y} \mid \Omega) - \frac{1}{2} \log(|\nabla^2[\text{vec}(\hat{\mathbf{H}}_{\Omega})]|) \\ &+ \lambda \times [\log p(\rho_{\text{base}}) + \log p(\rho_{\text{disrupt}}) + \log p(\sigma_{\text{base}}) + \log p(\sigma_{\text{disrupt}})]. \end{aligned}$$

To aid in model identification, we also imposed the constraint  $\sigma_{\text{base}} < \sigma_{\text{disrupt}}$ , assuming greater variation is attributed to the starvation kernel following prior reports ?. Finally, we set  $\rho_{\text{base}} > \rho_{\text{disrupt}}$ , reflecting the expectation that, in the absence of starvation, the base kernel should exhibit smoother and flatter trends. Note that we did not center the posterior samples at a mean of 0, as no intercept was included in the model. We chose  $\lambda = 120$  which was the smallest value of that was able to identify the distinction between  $\mathbf{f}^{(\text{disrupt})}$  and  $\mathbf{f}^{(\text{base})}$ . No perceptible change in estimated disruption effects was observed for values between 120 and 200.

## 7 Details on Lifestyle microbiome data

We describe the application of MultiAddGPs to the longitudinal microbiome dataset. Compared to the artificial gut data, this study involves a simpler model structure with only one single time series. However, it still captures two overlapping temporal processes: a general long-term trend,  $\mathbf{f}^{(\text{trend})}$ , and a travel intervention effect,  $\mathbf{f}^{(\text{travel})}$ , which induces rapid microbiome fluctuations. The time series was standardized to have a mean of zero and a standard deviation of one before model fitting. All kernel mean functions were set to zero, and both temporal components were modeled using squared exponential kernels:

$$\begin{aligned}\mathbf{\Gamma}^{(\text{trend})} &= \sigma_{\text{trend}}^2 \exp\left(-\frac{(t_n - t'_n)^2}{2\rho_{\text{trend}}^2}\right), \\ \mathbf{\Gamma}^{(\text{travel})} &= \sigma_{\text{travel}}^2 \exp\left(-\frac{(w(t_n) - w(t'_n))^2}{2\rho_{\text{travel}}^2}\right).\end{aligned}$$

Here,  $w(t_n)$  is a transformed skewed Gaussian of input  $t_n$ , designed to capture the non-stationary nature of the travel intervention. Specifically:

$$\begin{aligned}z_n &= \frac{t_n - m}{s} \\ w_n &= \exp\left(\frac{1}{2}z_n^2\right) \times \frac{1}{1 + \exp(-\alpha z_n)}\end{aligned}$$

where  $m$  determines the peak location of the distribution,  $s$  governs its width, and  $\alpha$  is the skew parameter. When  $\alpha = 0$ , the function reduces to a standard Gaussian; a positive value of  $\alpha$  induces a heavier right tail, while negative value produce a heavier left tail. Here we set  $m = 92$ ,  $s = 20$ , and  $\alpha = 2$ . These choices effectively restrict the travel-related changes to a two-month window after the travel date, ensuring that the model captures the local, non-stationary fluctuations associated with travel without introducing undue influence at other time points.

For the kernel hyperparameters, we specified the following prior distributions:

$$\sigma_{\text{trend}}, \sigma_{\text{travel}}, \rho_{\text{travel}} \sim \mathcal{N}(5, 1),$$

$$\rho_{\text{trend}} \sim \text{InverseGamma}(10, 0.8).$$

This specification reflects prior knowledge from previous studies [?](#), suggesting that the long-term microbiome trend is more stable, while travel-induced changes exhibit greater variation and sharper fluctuations. In other words, the prior penalizes extremely small or large length scales. The penalized marginal likelihood is given by

$$\begin{aligned} \log \int p(\mathbf{H}, \mathbf{Y} \mid \Omega) d\mathbf{H} &\approx \frac{(D-1)N}{2} \log(2\pi) + \log p(\hat{\mathbf{H}}_{\Omega}, \mathbf{Y} \mid \Omega) - \frac{1}{2} \log(|\nabla^2[\text{vec}(\hat{\mathbf{H}}_{\Omega})]|) \\ &+ \lambda \times [\log p(\rho_{\text{trend}}) + \log p(\rho_{\text{travel}}) + \log p(\sigma_{\text{trend}}) + \log p(\sigma_{\text{travel}})]. \end{aligned}$$

To ensure model identifiability, we imposed the constraints  $\sigma_{\text{trend}} < \sigma_{\text{travel}}$  and  $\rho_{\text{trend}} > \rho_{\text{travel}}$ , reflecting the assumption that the travel-related kernel captures higher-frequency variation, while the general trend evolves more smoothly and gradually. The posterior distributions were centered at a mean of zero. The full set of posterior estimates for the bacterial family-level contributions of  $\mathbf{f}^{\text{trend}}$ ,  $\mathbf{f}^{\text{travel}}$ , and their cumulative effect  $\mathbf{f}^{\text{trend}} + \mathbf{f}^{\text{travel}}$  are presented in [Figures 7,8](#), and [6](#).

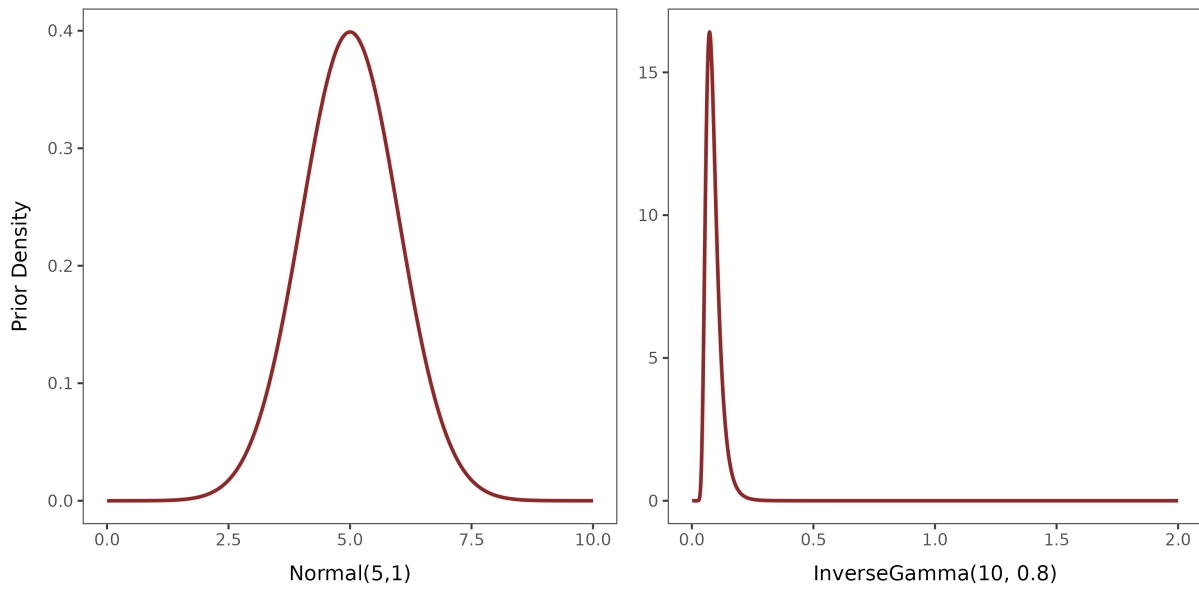


Figure 5: Prior density plots for the Normal and InverseGamma distributions used for the hyperparameters in the kernel functions (Longitudinal microbiome data).

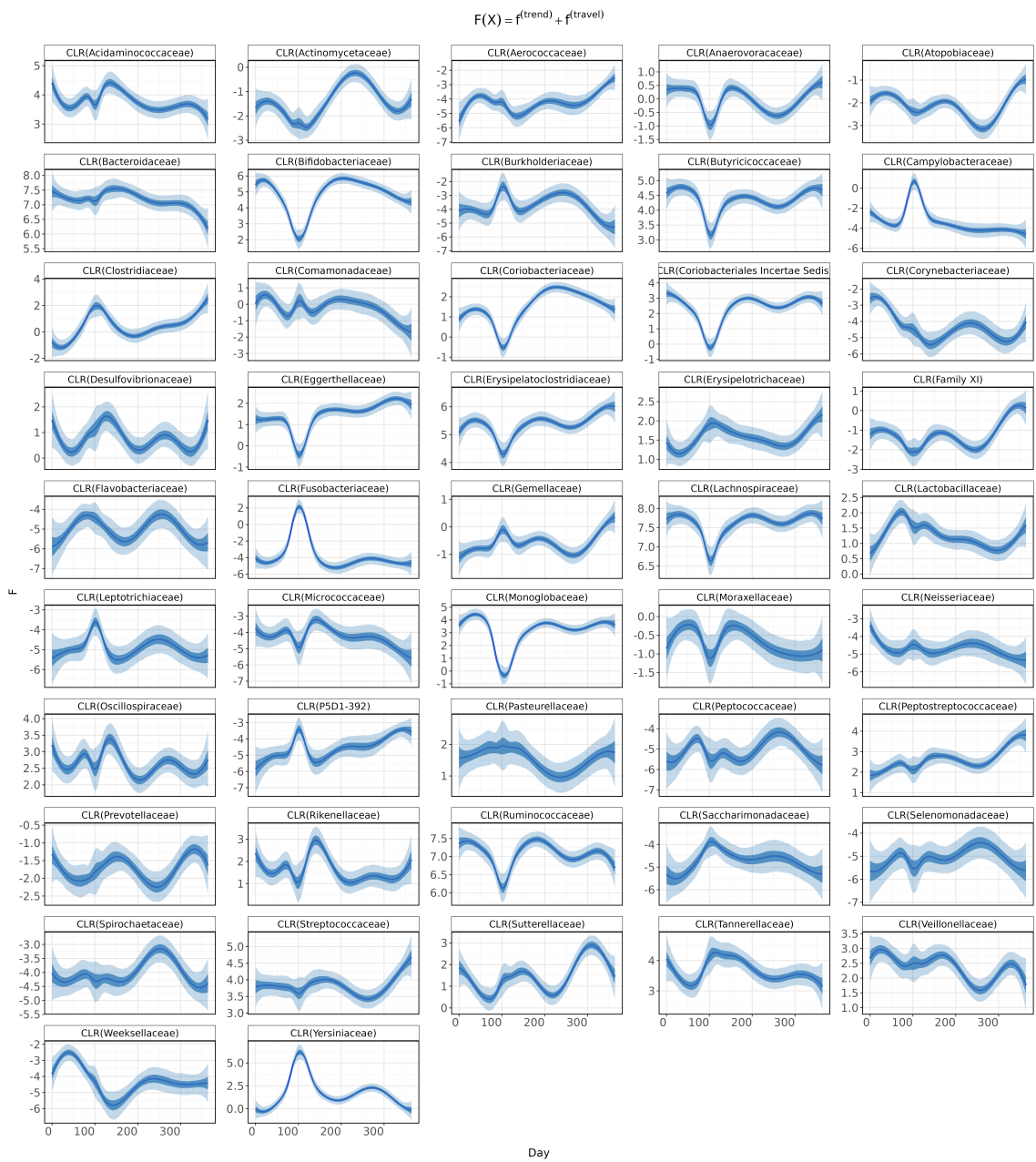


Figure 6: MultiAddGPs Posterior for the Smoothed State F in the Longitudinal Microbiome Study

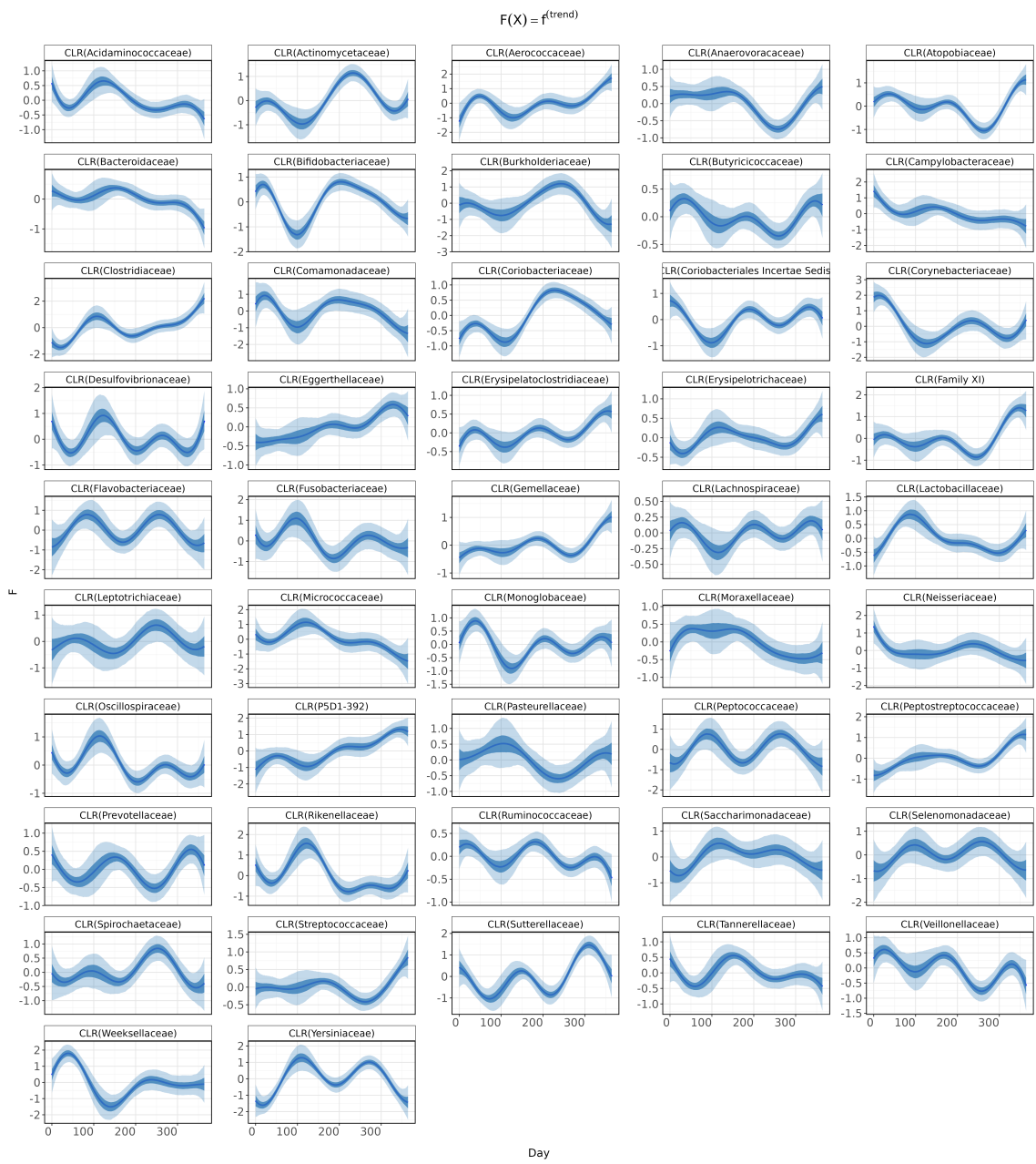


Figure 7: MultiAddGPs Posterior for the general trend effect  $f^{(\text{trend})}$  in the Longitudinal Microbiome Study

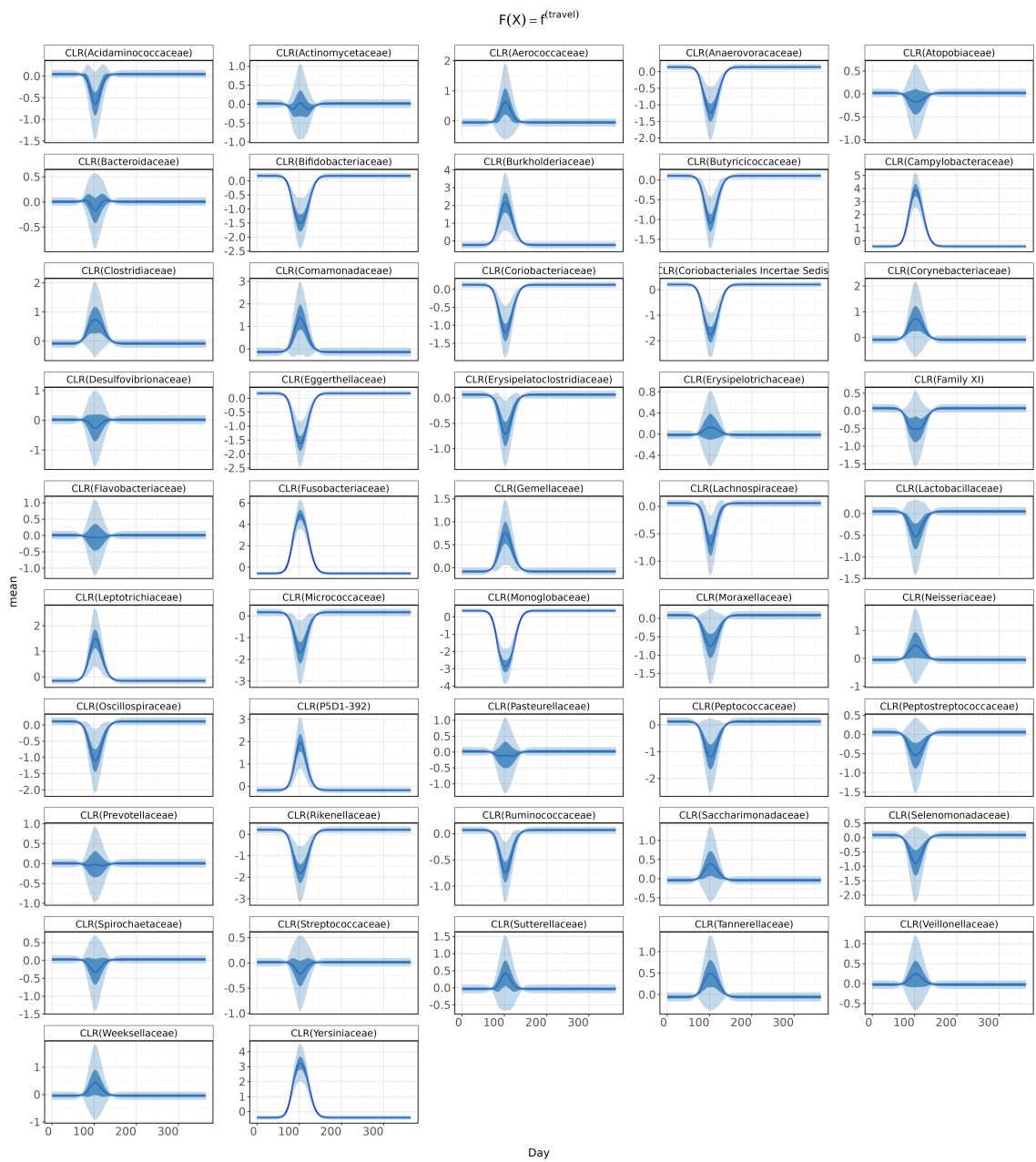


Figure 8: MultiAddGPs Posterior for the travel intervention effect  $f^{(\text{travel})}$  in the Longitudinal Microbiome Study